Analysis of IR-806 Aggregation and Chromonic Liquid Crystal Properties

By: Elizabeth Mills
Advisor: Peter Collings

March 14, 2011

Abstract

IR-806 is an infrared absorbing chromonic liquid crystal that forms a liquid crystal phase at around 0.45 wt% at room temperature. It has a unique coexistence region whereby there is not ever a distinct separation of phase between the isotropic liquid and liquid crystal regions, only a decrease in birefringence everywhere. Also, IR-806's most stable conformation (in gas form) was obtained, and it was found to be most stable in its AA conformation. Unfortunately, it was discovered that IR-806 is not stable in solution, quickly degrading in acidic environments, and not completely stable in any aqueous environment. The decay times of a 0.0005 wt% solution were 21 $\pm$ 1.6 hours at pH 2.8 and 108 $\pm$ 1.6 hours at pH 7.3. It is least stable at low concentrations, but was also found to degrade in solution at liquid crystal phase concentrations.

IR-806 exhibits a very dynamic absorption spectra, with three distinct peaks that vary in amplitude depending on concentration. These peaks can be connected to the formation of different aggregate species in solution as concentration changes. Analysis of these peaks support the idea that there is a distinct structural change between the aggregates before the liquid crystal phase. Analysis of the low concentration peak amplitude (or monomer peak) allowed for a calculation of stacking free energy change. IR-806 was found to have a stacking free energy change of 9.01 $\pm$ 0.12 k_BT.

Although it may not have long term applications due to its instability in solution, IR-806 might be able to shed light on how other chromonics aggregate at concentrations lower than their liquid crystal phase. This report discusses the investigation of such chromonic and liquid crystal properties not only with the purpose of learning more about IR-806, but also of applying this insight to other chromonic liquid crystals.

Contents

Chapter 1

Introduction

1.1 The Phases of Matter

Since the beginning of our scientific exploration and introduction, we have learned to categorize matter into three phases. Depending on the surrounding temperature and pressure, a substance exists as either a solid, a liquid, or a gas. The molecules comprising a substance move differently depending on the material's phase.

In solid materials, molecules hold positional order, meaning that each remains stationary relative to all other molecules in the material. Frequently, this positional order is accompanied by orientational order, whereby the molecules align, on average, along a common axis, forming a repeating pattern of atoms, or lattice, within the material. We commonly interact with many examples of solid lattices, such as salt, sugar, and ice.

When matter is in the liquid phase, it maintains no positional or orientational order. For example, when ice melts into liquid water, its rigid lattice breaks into randomly oriented H_2O molecules, with fleeting bonds made and broken on the order of nanoseconds. For example when a cube of ice melts into liquid water, it maintains some positional order, and no orientational order. While the molecules within a liquid do experience attractive forces that keep them near to one another, they are free to move around and tumble, with no preferred direction for alignment. This is why water can be contained in an open glass upon the table, but spills out in a unified stream when the glass is knocked on its side. The molecules within a liquid are free to move, but they must move together.

In contrast, the gas phase is defined by the complete absence of both positional and orientational order among its molecules. In the gas phase, a material expands to the volume of its container, and its molecules only weakly interact with one another. Thus, gaseous materials generally exist at lower densities, and are generally invisible to us. We interact with gases in a much less tangible way than we do with liquids and solids, and frequently take for granted the unique combination of molecules that comprise the air we breathe.

Because the molecular freedom that defines these phases depends on the external temperature and pressure, a change to the external environment can induce a phase transition within a material. We are familiar with the phase transitions of water through common

events. For example, melting ice dilutes a fountain soda, evaporated water steams out of a boiling tea kettle, and atmospheric water vapor wets a tabletop as it condenses around the bottom of a cold glass. Moreover, while a phase transition does change material properties, it is not considered to be a chemical reaction. This is because the fundamental molecular structure comprising a material remains constant, independent of its phase, and phase transitions merely alter the overall movement and *inter*molecular bonds among the molecules. Ice, steam, and liquid water are all comprised of the same molecule, H_2O. [1]

1.2 The Liquid Crystal Phase

This overview of the solid, liquid, and gaseous states was believed to describe all the phases of matter until the late 1880's, when it was discovered that, within a particular temperature range, some materials couldn't be characterized as either a solid or a liquid because they contained hybrid qualities of the two phases. These materials were initially discovered when a material in a solid lattice was heated enough to destroy its molecules' positional order, but keep some of their orientational order. Physically, the "melted" material maintained a cloudy appearance, resulting from the molecules' preserved uniform preferential direction of alignment. When this cloudy phase continued to be heated, its appearance eventually cleared, with a significant reduction in its viscosity. This final state described the usual qualities of the material in its liquid phase. However, at that time, the intermediate state was an entirely unknown phase of matter.

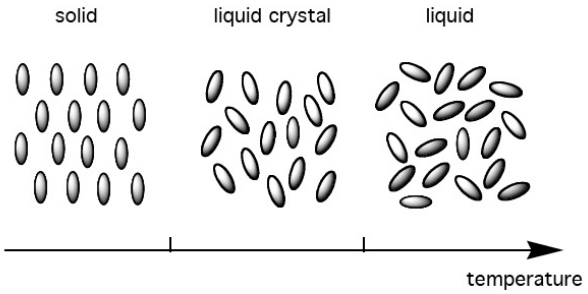

Figure 1.1: Molecular alignment is compared between the solid, liquid crystal, and isotropic liquid phases. A solid has both positional, and frequently, orientational order, while a liquid has none of this order. A liquid crystal has an intermediate amount of order, with some orientational order, and, occasionally, positional order. Note that not all the liquid crystal molecules are aligned the same way. Rather, there is a preferred direction for molecular alignment over a *time average*. [1]

This fourth phase of matter is now called the liquid crystal phase, and indeed results when fluid matter retains orientational order and even sometimes positional order. Some materials become a liquid crystal at temperatures between their solid and liquid phases; in this phase they maintain the fluid nature of liquid while maintaining structure in molecular orientation. Figure 1.1 shows a schematic representation comparing molecular order in the solid, liquid crystal, and liquid phases. Because most of the energy contained in a lattice results from

positional structure, a solid to liquid crystal phase transition requires substantially more energy than a liquid crystal to liquid phase transition does. Thus, a material in its liquid crystal phase is much closer in energy to a liquid than a solid, and, aside from the properties due to its degree of orientation order, the liquid crystal phase is analogous to the liquid phase. I like to think of the structure of the "crystal" as an adjective modifying the noun of the fluid "liquid." In this perspective, whatever properties differ between liquid crystals and liquids arise entirely from a time averaged preferred direction for molecular orientation.

It took many years after the discovery of the liquid crystal phase for scientists to see that the preferential molecular orientation, or anisotropy, of the liquid crystal phase had practical applications. Due to their fluid yet structured nature, materials in the liquid crystal phase are affected by slight changes in their external environment, whereby molecular alignment can shift in response to applied stress, heat, or electric field. Also, the anisotropic nature of a liquid crystal changes the polarization of light, such that polarized light can be transmitted through *crossed* (perpendicular) polarizers when a liquid crystal cell is placed between them. This property, known as birefringence and discussed more in Chapter 2, is the crux of liquid crystals' current application.

In the late 1950's work began in an effort to apply this sensitivity to technology, and in the early 1970's the first liquid crystal display (LCD) was constructed as a way to read a digital watch. Today LCD's are an integral part of our productivity *and* entertainment as the intricate color display comprising flat computer and television screens. In one type of LCD screen, called a vertical aligned device (VA), there are many cells that can, individually, be turned on by means of applying a voltage through them. Each cell is set up such that a thin layer of liquid crystal material between two pieces of glass is then placed between crossed polarizers. A beam of light then shines through the material, perpendicular to the surface. Also, a surfactant material is incorporated into the glass/liquid crystal interface, so that the liquid crystal's director (preferential direction of alignment) is parallel to the light beam. As such, there is no component of any light polarization parallel to the director, and no birefringence occurs. Because no birefringence occurs, no light polarization is changed, all light is extinguished between the cross polarizers, and the cell appears dark. To make the cell light up, a voltage is applied across the cell, also parallell to the direction of the light propagation. The type of liquid crystal in this cell is such that it changes its alignment to be perpendicular to the direction of the resultant electric field. Because the electric field is parallel to the direction of the applied voltage, it is also parallel to the original alignment of the liquid crystals. This changes the director such that it now has a component *parallel* with the *light's polarization*, which induces birefringence and makes the cell light up. Several of these cells comprise each pixel of a monitor or screen, so that we are able to see such vibrant colors. [2]

1.3 Lyotropic Liquid Crystals

So far, we have discussed a material's liquid crystal phase as arising in a temperature region that gave its molecules enough energy to exist in a state between their solid and liquid

phases. However, some materials can form a liquid crystal phase when dissolved in *solution*, where solution concentration plays a dominant role, with temperature, in determining the structure and stability of the phase. The temperature dependent liquid crystals present in LCD technology are categorized as thermotropic, while concentration dependent liquid crystals are called lyotropic liquid crystals. [1]

Lyotropic liquid crystals exist commonly around us in many forms, and it is the amphiphilic, or both water loving and fearing, nature of such molecules that creates ordered structures within the solution. Both soap molecules in detergents and phospholipid molecules within cells form lyotropic liquid crystals when dissolved in water above a concentration threshold, called the critical micelle concentration. Figure 1.2 shows an example for the molecular formula of a soap molecule, along with a the shape of a micelle, the aggregate structure that soap molecules form when the concentration exceeds their critical concentration. From a practical perspective, detergent micelles form around dirt molecules to help dissolve them in water and remove them from fabric.

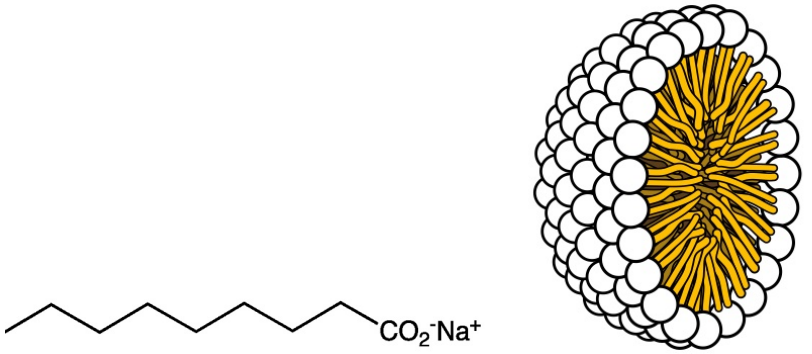

(a) Soap Molecule (b) Micelle

Figure 1.2: Example soap molecule and molecular structure of a micelle. A soap molecule has a polar head attached to one or more long nonpolar chains. Due to its strong amphiphilic nature, it can bond with both polar and nonpolar molecules simultaneously. When solution concentration exceeds the critical micelle concentration (unique to each type of soap), micelles form. The nonpolar tails cluster together in the center, while the polar heads interact with the surrounding water. Courtesy of Wikipedia.

The molecules' polar heads are attracted to surrounding water molecules, while their nonpolar tails cluster themselves to the middle, forcing out all solvent from the interior. These amphiphilic interactions create the overall spherical shape of the micelle, where the polar heads comprise the outer shell.. Amphiphilic substances are also known as surfactants because their structures allow them to act as a buffer, or separation, between polar and nonpolar substances. They can create a homogenous, or uniform, solution out of normally immiscible liquids. It is soap's surfactant nature that allows water to "dissolve" oil and grease off of dishes and out of clothing. When other fatty molecules are present in solution with soap molecules, they are attracted into the center of these micelles, where they can avoid the polarity of the external environment. In this way, nonpolar molecules can "dissolve" in

water, with soap as the cleaning agent. [3]

Figure 1.3 shows an example of a molecule, first as a single molecule and then, schematically, as part of a large phospholipid bilayer sheet. This liquid crystal structure comprises the cell membrane that separates the cell's internal and external environment, and coats many internal structures within the cell.

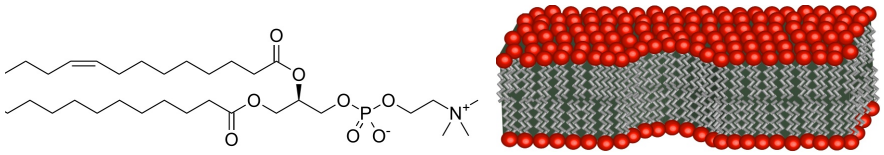

(a) Phospholipid Molecule (b) Phospholipid Bilayer

Figure 1.3: Example phospholipid and bilayer molecular structure. Courtesy of Wikipedia.

A phospholipid has amphiphilic character similar to a soap molecule, except that the polar head contains a phosphate group, followed by multiple fatty tails. A phospholipid bilayer requires two phospholipid layers so that a polar environment can exist both within and outside a cell. Naturally, it takes a larger concentration of the molecule in solution to be able to produce this bilayered structure, and, at concentrations below this threshold, phospholipids form vesicles. A vesicles has a spherical structure similar to a micelle, except that the outer shell is comprised of a bilayer. This means that an aqueous environment exists both inside and outside vesicles. [4]

Research on these lyotropic liquid crystal phases has drastically changed the surfactant industry, enhancing the quality of detergents, creams, makeups, and other foaming agents. In addition, recent insights about cell membrane stability and structure have important medical applications, and synthesized bilayer structures can be used on the nano scale for drug delivery and solubility within the body. [1]

Because soaps and phospholipids are rodlike and extremely amphiphilic in character, their liquid crystal structures generally maintain spherical symmetry, as alternating polar and nonpolar spherical shells. This makes the macroscopic composition of the material isotropic, and, as such, there is no birefringence to alter light polarization. Therefore, such liquid crystals rarely have optical applications like thermotropic liquid crystals do. The field of lyotropic liquid crystals was all but set aside by the optical industry, until the 1980's, when a special class of anisotropic lyotropic liquid crystals was discovered that blended both optical and medical applications.

1.4 Chromonic Liquid Crystals

This unique class of material is called the lyotropic *chromonic* liquid crystal (LCLC) because it generally exists as a dye that absorbs visible light when dissolved into solution. These molecules are disk-shaped and less amphiphilic, consisting of a flat aromatic backbone with polar groups extending along the periphery or as side chains. Hydrophobic interactions,

along with weak attractions between aromatic rings of different molecules (called π bonding) create a preference for molecular stacking. Because this stacking can occur with any number of molecules, aggregation can begin at any concentration, and many chromonic liquid crystals do not appear to exhibit the equivalent of a critical micelle concentration. Such aggregation (discussed more in Chapter 2) is called isodesmic because it occurs at all concentrations. However, the aggregates formed at low concentrations are not large enough to align, and, at larger concentrations, aggregate size increases into supramolecular assemblies. The exact size of the aggregates is concentration dependent, and birefringence only occurs when it is energetically favorable for the aggregates to orient themselves in a uniform direction, which requires them to be sufficiently large. Such birefringence is the first sign of the liquid crystal phase. [5] Figure 1.4 shows a schematic representation of chromonic molecules forming small unaligned aggregates at a low concentration and larger, aligned aggregates at a high concentration. For lower concentrations and/or higher temperatures, some aggregates exhibit a preferred direction for alignment and others remain randomly oriented. At this stage, the chromonic is in its isotropic liquid and liquid crystal coexistence phase, and this region can span a range of concentrations and temperatures. However, at a given temperature, each liquid crystal has a unique upper and lower concentration that sets its coexistence region. Generally, this coexistance region is apparent by groups of similarly aligned aggregates (domains) melting together. By convention, a material is not considered completely in its liquid crystal phase until all of its domains are aligned.

(a) Low Concentration (b) High Concentration

Figure 1.4: Chromonic Aggregation into the Liquid Crystal Phase. At low concentrations, aggregates form but are not densely populated enough to align. At high concentrations the randomly oriented aggregates start bumping into one another, and it become more energetically favorable for them to align along the same direction.

Chromonic liquid crystals are just like other lyotropic liquid crystals in that their molecules are still free to move around, even when they are part of a larger aggregate that is aligned with other aggregates. The molecular organization exists over a time average, where individual molecules can leave one aggregate and re-enter into another, such that the structure remains overall constant. The driving forces behind such chromonic alignment result from non-covalent, reversible bonding among the aggregates. Such bonding is thought to arise from dipole-dipole interactions, hydrogen bonds, and hydrophobic forces.

For a given temperature, there is an associated concentration where aggregate alignment begins to occur; each type of chromonic dye has a unique temperature and concentration

dependence for its liquid crystal formation. Chromonics align at a lower concentration when their molecules experience a greater attractive force between one another, compared to the surrounding H_2O molecules.

Recent investigation has shown that some chromonics form their liquid crystal phase at concentrations of 6-30 wt% while others transition at concentrations as low as 0.3-0.5 wt%. Examples of the former category are disodium cromyoglycate (DSCG), Sunset Yellow, and Bordeaux dye, two of which have structures shown in Figure 1.5

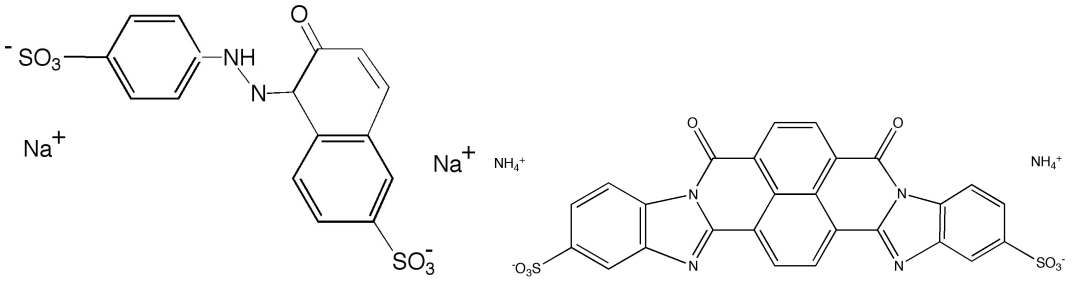

(a) Sunset Yellow Molecular Structure (b) Bordeaux dye Molecular Structure

Figure 1.5: Structural formulas for two types of chromonics that form a liquid crystal phase at higher concentrations. Sunset Yellow and Bordeaux dye transition at concentrations of 30 and 6 wt%, respectively, at room temperature.

The latter category surprisingly creates a more viscous liquid crystal solution, even though there is a lower concentration of molecules in solution. It is theorized that the dye incorporates water molecules into the aggregate structure. A chromonic's ability to form a liquid crystal phase at lower concentration is attributed to a more favorable change in energy from aggregate formation. This driving force is quantified as a "stacking free energy change," or stabilizing loss in energy by moving a molecule in solution into the interior of an aggregate stack. Two examples of low concentration chromonics are pseudoisocyanine chloride, known as PIC, and benzopurpurin 4B, known as BPP. Their chemical structures are shown in Figure 1.6.

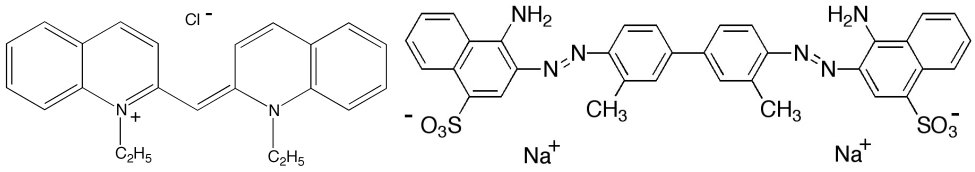

(a) PIC Molecular Structure (b) BPP Molecular Structure

Figure 1.6: Structural formulas for two types of chromonics that form a liquid crystal phase at low concentration. PIC and BPP transition at concentrations of 0.3 and 0.5 wt%, respectively, at room temperature.

Both enthalpy and entropy are hypothesized to drive such chromonic aggregation, which

is different than the purely entropic hydrophobic interactions that drive non-chromonic soap and phospholipid aggregation. Table 1.1 displays the liquid crystal properties of previously studied chromonics, including this stacking free energy change. In addition, it shows the liquid crystal onset concentration at room temperature and the aggregate cross-sectional diameter in units of each dye's molecular diameter, respectively.

Table 1.1: Liquid Crystal Properties of Previously Studied Chromonics [5]

Chromonic	c_{onset} (wt%)	$D_{\text{aggregate}}/D_{\text{mol}}$	$\Delta\mu/k_BT$
DSCG	11	2	7.1
Sunset Yellow	30	1	7.2
Bordeaux Dye	6	2.5	9.2
BPP	0.5	unknown	10.3

Both types of chromonic liquid crystals are very interesting, due to the strong temperature dependence of their aggregation properties. Ultimately, it is the liquid crystal phase that provides technological applications, but understanding the stability and composition of aligned aggregates requires knowledge about aggregate formation. Also a dye's electronic properties change from low to high concentrations. The process of building larger aggregates is frequently observed through changes in the material's absorption spectra. As monomers and small aggregates bond together into the formation of a larger aggregate, the electronic properties of the material change and it begins to absorb light at different wavelengths. Observing changes in absorption spectra can be a reliable way to quantify how concentration affects aggregate formation.

When chromonics aggregate, new material properties emerge that are entirely different and seemingly unrelated to the properties associated with the single molecule. [6] This is because aggregation results from weak bonding between multiple molecules, whereby electronic configurations and electromagnetic absorption properties are changed from "near-neighbor" effects. In the same way that aggregates align from intermolecular attractions, aggregates are formed from non-covelant bonding between the individual molecules, in stark contrast to the covalent bonding that comprises individual molecules themselves. As such, intermolecular bonding can result from practically any reversible interaction between the molecules that allows a single molecule, as its own entity, to detach itself from an aggregate stack, whereby another molecule can takes its place. The molecular stacking that creates most chromonic aggregate structures occurs by means of $\pi-\pi$ bonding, dipole-dipole forces, hydrogen bonds, and/or hydrophobic interaction.

In $\pi-\pi$ bonding, the aromatic cyclic groups that comprise the backbone of chromonic molecules create a reduced electron density by the hydrogens around their perimeter. The positively charged hydrogen atoms can enhance their exposure to electron density by lining up either above or below another molecule's aromatic configuration, slightly offset from one of the carbon atoms. The hydrogen atom can then interact with one of carbon's π orbitals

and additional $\pi - \pi$ intermolecular orbital bonding can ensue between carbons from both molecules. As such, electron rich and electron poor areas balance one another and the flat aromatic structures have a driving force for stacking. Also, the aromatic backbones prefer to be distanced from a polar solvent, so chromonic dyes dissolved in water (the usual solvent) have an additional driving force for aggregation. The hydrophobic interactions are probably not as important as they are in other lyotropic molecules, like the phospholipids and soap molecules, but they do enhance stacking free energy changes. [6]

Likewise, dipole-dipole interactions are also driving forces for the aforementioned lyotropics. When hydrophobic effects are at play between nonpolar hydrocarbons and the water in solution, so too are the *polar* components of the hydrocarbon attracted to the water molecules. In chromonics, the conjugated systems in the interior are often attached to polar chains at the ends of the molecule. Referring back to Figures 1.5(a), 1.5(b), and 1.6(b), SunsetYellow, Bordeaux dye, and BPP all have polar ends consisting of sulfonyl (-SO_3) groups. These ends undoubtedly interact with surrounding water molecules (and probably each other) in such a way that the aggregates keep these polar groups along the periphery and separate like charges from one another. In the case of Bordeaux dye, it is hypothesized that, because the negatively charged sulfonyl groups repel one another, the molecules are slightly offset and rotated from one another between stacking layers. However, Sunset Yellow has been found to have a simpler aggregate structure consisting of a cross-sectional area of a single molecule, even though it, too, has sulfonyl groups. Clearly, there are unanswered questions.

Lastly, whenever water is a solvent, there are always hydrogen bonds. Although they do not usually interact with the backbone structure of a chromonic molecule, hydrogen bonds can occur along the periphery. Hydrogen bonds are a special kind of dipole-dipole interaction, about ten times stronger than the usual dipole bond, where the hydrogen atoms in water molecules are attracted to electronegative atoms (having a high affinity for gaining additional electrons) in other molecules. Usually, hydrogen bonding occurs between hydrogen and either oxygen, nitrogen, or sulfur atoms. In fact, hydrogen bonds are the bonds that add additional strength to water molecules when water is in its solid lattice and liquid phase. The definition of water's phase transition to its gaseous phase is when it has enough energy to entirely break the hydrogen bonds between its molecules. [6] When electronegative atoms are part of a chromonic's molecular structure, water molecules may bond to the periphery of an aggregate and increase its stability. This may occur in the case of DSCG. Moreover, the nitrogen atoms *within* PIC and BPP may allow for hydrogen bonding *within* the interior of the aggregate. This could explain why aggregate formation occurs at lower dye concentrations and allows for the possibility of additional complexity in aggregate structure and aggregation mechanism.

Another way to learn about aggregates is by analyzing the effect of salt on their formation. It has been found that chromonic aggregation is enhanced by the presence of additional cations (positively charged atoms) in solution. Changing the concentration and specific type of cation has a significant effect on lowering the onset concentration and increasing the onset temperature for the liquid crystal phase. However, changing the anion (negatively charged

atom) composition does not affect the phase. This means that the dye's counter ion most likely plays a role in aggregate formation, and is probably incorporated into the aggregate structure. Research has additionally shown that sodium ions, the standard counterion in its synthesis, appear to have the optimal size for enhancing DSCG aggregation. [7] Most chromonics exist in solution as negatively charged, so their polar ends would be attracted to positively charged molecules and atoms in solution. The exact nature of how salt enhances aggregation is a complicated issue, as ions bond to water molecules in the form of hydration, where one charged atom can attract between six and eight water molecules around it at a given time. If there is a strong enough driving force, the cation can separate from the surrounding water molecules and replace them for its bond with the aggregate, but in conditions where weaker bonding occurs, the cation might very well be able to bring the water molecules with it when it bonds within the aggregate structure.

Interestingly, some chromonic dyes maintain the same general absorption spectra throughout their aggregation process, while others have absorption spectra that change dramatically as concentration changes. PIC is such a chromonic whose absorption peak shifts to higher wavelengths and drastically narrows when its concentration is increased past a critical threshold. [1] This absorption shift correlates with the formation of the large aggregates that, at a slightly higher concentration, align into their liquid crystal phase.

Another difference found between various chromonics is the cross sectional area of their aggregates, included in Table 1.1. X-ray diffraction experiments have shown that higher concentration chromonic liquid crystals have aggregates whose cross sectional area ranges from 1 to 6 molecular areas. Sunset Yellow was found to have an aggregate cross-sectional area of only a single molecule, while Bordeaux dye was found to have an aggregate area of 2.5 molecules. [8]. From such aggregate cross-section results and comparisons with onset liquid crystal concentrations, it seems that the formation of a liquid crystal at a lower concentration correlates with a larger cross-sectional area. Lower concentration liquid crystals appear to agree with this trend, but in a much more dramatic fashion. Both PIC and BPP, forming their respective liquid crystal phases around 0.4 and 0.34 wt%, were found to have cross-sectional areas much too large to measure using the x-ray diffraction technique. This suggests the aggregates are many molecules across, which supports the idea that water molecules might be involved in their aggregate structures. While the cross-sectional area of the aggregates varies between chromonics, a consistent displacement between stacked molecules has been found, equal to 3.4 Å. This is the same distance between base pairs in DNA and the spacing between single sheets of carbon atoms in graphite. [8]

New chromonic dyes are currently being discovered and synthesized, and known dyes are being studied to learn more about their fundamental properties, as there are many applications for such materials. One such application is a new type of polarizer, called an E-type, is different from the usual O-type polarizer because it absorbs light with polarization *perpendicular* to the optic axis (as opposed to parallel the parallel). The polarizer is produced by putting a thin layer of aligned chromonic liquid crystal solution on top of a surface and evaporating the water off. The chromonic aggregates maintain their orientation and the resulting material is a thin film that is used as the polarizer material. Such chromonic films

can also be used as optical retarders because they highly retard light with wavelength in the vicinity of their peak absorption.

From the combination of their delicate aggregation and aqueous environment, chromonic liquid crystals also have biomedical applications. Chromonics, placed between crossed polarizers, can be used to detect the formation of immune complexes, because the structural growth from antibody-pathogen binding among aggregates disrupts their alignment. [5] In the same way that LCD technology "turned on" light through crossed polarizers by changing the liquid crystal alignment, so too can antibody-pathogen binding act as a disturbance that redirects some aggregates such that they are no longer oriented parallel to one of the polarizer axes. If a different type of antibody is injected into each cell of a large grid, and every cell is already full of a blood sample in combination with an aligned chromonic, the blood sample could be analyzed by observing which cells suddenly lit up from an immune complex disturbance.

The phase transitions of chromonics are currently an exciting area of investigation, whereby slight temperature and concentration changes create transitions between the liquid crystal and isotropic liquid phases. Furthermore, an additional transition can occur between multiple liquid crystal phases. The liquid crystal phase that arises from the isotropic liquid phase transition is called the nematic (N) phase. It contains only orientational order between its aggregates and maintains less order than other liquid crystal phases. However, at a lower temperature (or possibly a higher concentration), chromonics can transition from an N phase to a hexagonal (M) phase, which possess positional order in addition to orientational order. [9] Figure 1.7 shows schematic representations of stacking in the N and M phases, respectively. In most cases, only the chromonic N phase is observed, as we are primarily observing phase transitions from the isotropic liquid phase.

In all, it is important to investigate aggregate structures and the processes, mechanisms, and characteristics involved with the aggregation process. There is currently a vast amount of information regarding chromonic phase transitions and birefringence, but researchers are just beginning to propose and test theories about chromonic aggregation.

1.5 Near-Infrared Absorption and IR-806

A new area of research combines chromonic liquid crystal research with near-infrared (NIR) absorbing materials. IR-806, an NIR absorbing dye recently synthesized from croconium, expands chromonic absorbing properties to the infrared. It's original use was for biological tagging, as infrared radiation is gentler on cell protein and living tissue. Many IR-absorbing dyes are currently used for biomedical research and in industry, but IR-806 is, so far, the only IR absorbing dye found to create a chromonic liquid crystal phase, specifically between the concentrations of 0.4-10 wt%. [10] The chemical structure of IR-806 is shown in Figure 1.8.

IR-806 is so named because its single absorption peak was originally found to sharply maximize at 806nm, completely in the NIR. However, current sources have cited the peak

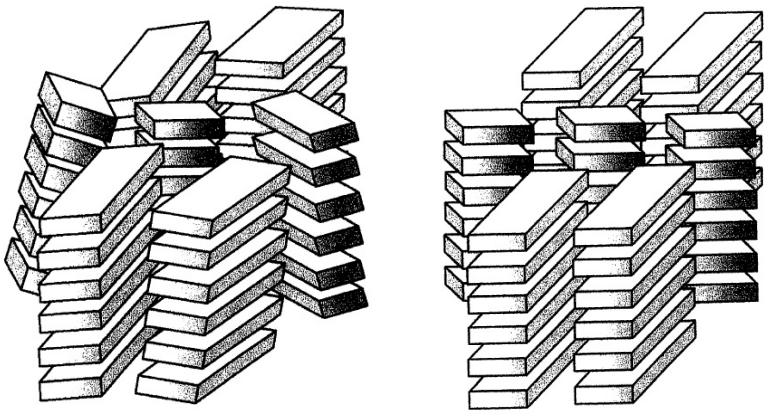

(a) N phase (b) M phase

Figure 1.7: Schematic representations for nematic (N) and hexagonal (M) phases in chromonic columnar aggregate stacking. As can be seen, the stacks in the M phase arrange into a hexagonal lattic. This shows greater positional order than the N hphase aggregates, which have only a preffered orientation for alignment. [9]

to exist at around 800nm, not specifying it exactly. If IR-806 indeed aggregates into a chromonic liquid crystal phase, then these discrepancies regarding its absorption spectra may occur because IR-806's absorption spectra depends on its concentration in solution. In previous experiments, IR-806 has been observed to remain soluble in water, which supports the notion that IR-806 can be used like other chromonics,and possibly have biomedical applications through its NIR absorbing properties. [11]

Even more importantly, further investigation of IR-806 can yield information about its specific chromonic nature. Its low concentration liquid crystal phase formation puts it into a similar chromonic category as PIC and BPP. If IR-806's absorption spectra does show a sharp spectral shift like PIC, then information can be gained regarding IR-806's aggregation mechanism. What we learn about IR-806's aggregation mechanism might then be able to be applied to aggregation mechanisms in general, and perhaps we can learn more about the chemical processes that allow for single dye molecules to self assemble into supramolecular aggregates.

Also, just by looking at IR-806's molecular structure, one can hypothesize the particular interactions that might contribute to its stacking nature. Referring back to Figure 1.8, one could hypothesize that IR-806's conjugated chain could provide a backbone structure for stacking similar to DSCG and Bordeaux dye. However, IR-806 does have polarity within its backbone (the nitrogen and chlorine atoms), which could attract water molecules into its aggregate structure, as hypothesized for BPP aggregates. IR-806 also has sulfonyl groups on its edges, attached to long butyl chains, which might also interact with each other and water molecules in solutions just like Bordeaux dye and BPP. Moreover, IR-806 is unique from all the other chromonics (except PIC) in that it is a zwitterion, meaning it has an ionic

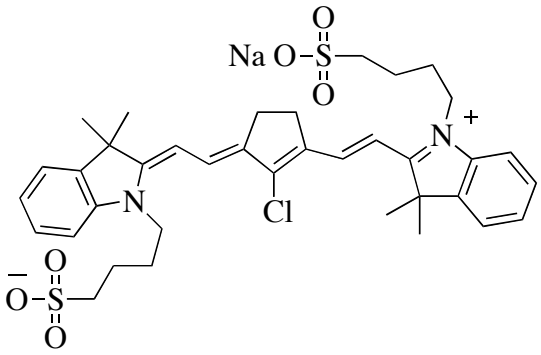

Figure 1.8: IR-806 Structure

separation of charge *within* its molecular structure. Both PIC and IR-806 have resonance structures that shift the positive charge back and forth between the two nitrogens, but IR-806 is the only chromonic that also has negatively charged end groups. Therefore, it is likely that IR-806 shares some features with PIC, while showing other qualities similar to Bordeaux dye or BPP.

Experimentation with IR-806 follows similar procedures as past research on other chromonics. It is necessary to learn about its liquid crystal phase onset concentration and how it varies with temperature. With this information, a phase diagram can be constructed that determines IR-806's phase for a given temperature and concentration. The phase diagram can also help us predict trends for IR-806 phase stability. Also, IR-806's absorbance spectra must be carefully analyzed through a wide concentration range, spanning the lowest detectable concentrations in solution through concentrations where aggregates are aligning into their liquid crystal phase. Changes in this absorption spectra can be linked to relative populations of differently sized aggregate structures in solution, and may ultimately provide the necessary information to construct viable aggregation mechanisms. However, before these mechanisms can be produced, we need to understand the exact sizes of these aggregates and the number of IR-806 molecules that comprise them. Moreover, IR-806, like other dyes, can exist in different conformational states, and different conformations could produce different aggregate structures and aggregate tendancies.

Lastly, experiments with x-ray diffraction, dynamic light scattering, and magnetic-induced birefringence can provide information about aggregate stacking, size, stability, and dynamics in solution. While some sources have claimed IR-806 is stable in solution, other sources have observed relatively fast absorbance decay for low concentration solutions. Therefore, it is also important to test this stability and determine what factors, if any, are responsible for this degradation. Hopefully, investigation of IR-806 through these techniques will show some interesting properties that provide additional insight into aggregation and the unique liquid crystal phase of chromonic dyes.

Chapter 2

Theory

2.1 Investigation of Most Stable Conformation

Because molecular stacking intrinsically depends on molecular structure, it is important to properly depict IR-806 on the molecular level. Figure 1.8 is the chemical formula provided by Sigma Aldrich, its manufacturer. While this structure is an easy way to depict IR-806, it might not necessarily correspond to the only conformation that IR-806 molecules adopt in solution.

In fact, IR-806 has three possible conformations due to bond rotations around the second carbon from the pentene ring. The alternating single and double bonds in IR-806 allow for the backbone to exist entirely conjugated, which allows for the positive charge to shift between the two nitrogens and the double bonds to shift over by one carbon in the direction of the positive charge. Through the interchanging of these two resonance structures, bond rotation is allowed around both C-C bonds exactly one carbon away from the pentene ring. These bonds are actually hybrids of a single and double bond, so at room temperature, although not constantly occurring, bond rotation is allowed.

As a result of this bond rotation, the nitrogens can either be flipped facing downward, closer to the chlorine atom, or flipped upward, away from it. Therefore, two other possible conformations exist (making a total of three), depending on how the two nitrogens align with the chlorine. Figures 2.1(a) and 2.1(b) show the structures of these other two possible IR-806 conformations.

Based on exactly where each nitrogen is located relative to the chlorine atom, these conformations have different names. Figure 1.8 is called an AS conformation because one nitrogen is syn to (on the same side of the molecule as) the chlorine, and the other nitrogen is anti to (on the opposite side of the molecule as) the chlorine. Similarly, Figure 2.1(a) and Figure 2.1(b) show AA and SS conformations. Because of molecular symmetry, these three structures account for all possible IR-806 conformations.

The most stable conformation of IR-806 is the one that minimizes electrostatic repulsions and provides the most stable geometrical relation among the atoms. Therefore, one can perform energy optimizations by iteratively solving the Schr"odinger equation for every

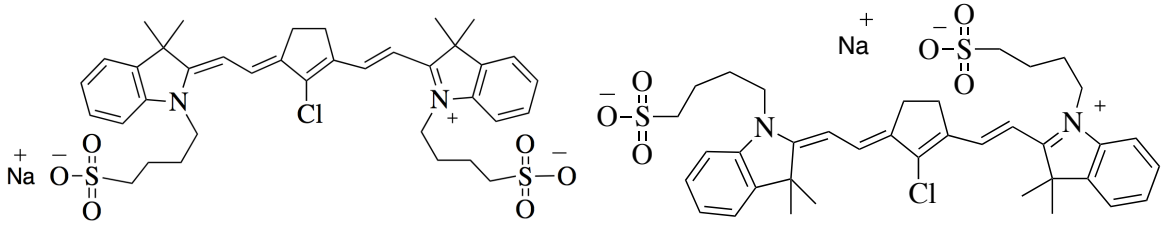

(a) SS IR-806 conformation (b) AA IR-806 conformation

Figure 2.1: Other possible IR-806 Conformations

electron and proton in the structure. As can be imagined, this is more easily said than done. First, since a molecule is an N-body system, there is no *exact* solution to its Schr"odinger equation, the best one can do is to solve it numerically with strategic approximations.

The nuclei in a molecule move on a much slower timescale compared to the electrons. Therefore, one can use the Born-Oppenheimer approximation to first calculate the total electrostatic energy of the system with the position of the nuclei held fixed. By choosing a particular level of theory and basis set of orbitals, the Shr"odinger equation is numerically approximated for each electron in the molecule. Then, using these fixed energies, one can geometrically optimize the position of the molecule's nuclei to obtain a better geometrical configuration (while ignoring the electrons). The electrostatics optimizations are called ab initio electronic structure calculations (AIESC), and they determine, for a given molecular geometry (and set of quantum mechanical approximations), what the most energetically favorable state is for each electron. Then, the geometrical optimization uses these energies to get the most favorable bond length, angle, and dihedral angle between the nuclei. [12] These processes create a feedback loop that could, in theory, continue infinitely. Realistically, however, hone chooses a set number of cycles based on how computationally taxing the particular structure is, and how long one is willing to wait for results.

IR-806 geometry optimizations were performed with the program Gaussian, using a B3LYP level of theory and 6-31G(d) basis set. [13, 14, 15, 16, 17] Because such energy minimizations account for every possible atomic orientation via stretching bond lengths and rotating bond angles, flexible chains provide too many degrees of freedom for the program to carry out results in a timely fashion. The iterative process of solving the Schr"odinger equation also sets an high polynomial relation between the number of atoms in the molecule and the time required to obtain a solution to the calculation. The combination of both these factors mandated the substitution of the two sulfonyl chains with methyl groups. It is believed that this substitution does not change the orientation or stability of the IR-806 backbone aromatic structure.

The results of the Gaussian calculations showed that the AA conformation existed at the lowest molecular energy. Table 2.1 shows the three lowest local energy minima, in both hartrees (H) and KJ/mole. Hartrees are the conventional unit for such conformation computations, and the "ZPE" is the energy in hartrees compared to the zero point energy obtained by performing the energy optimizations at 0 K. These calculations are all greater

Table 2.1: IR-806 Conformational Energy Minimization Results

Conformation	Energy (H)	ZPE (H)	Energy (kJ/mole)
AA	-1771.28823	0.57809	0.0
AS	-1771.28576	0.57819	7.1
SS	-1771.28329	0.57841	14.2

than the zero point energy because they are considered for room temperature. For the KJ/mole energy comparisons, only the relative energy difference between the conformations matters, so the lowest energy is set to zero and all other energies are shifted by that amount. In all, IR-806's relative enhanced molecular stability in the AA conformation translates to being 7.1 KJ/mole more stable than AS conformation, and 14.2 KJ/mole more stable than SS conformation. The majority of this stability stems from the elimination of steric hindrance between the methyl group attached to the nitrogen and the hydrogen on the carbon next to the pentene ring. Figure 2.2 shows a close-up of the molecular geometry when the nitrogen atom is syn to the chlorine atom.

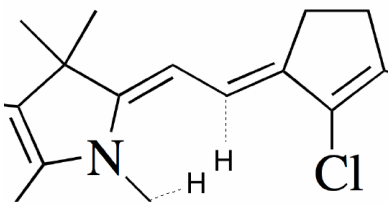

Figure 2.2: A close-up of IR-806 in anti orientation, showing steric hindrance between two hydrogens. The conjugated system requires that the backbone be flat, so the two hydrogens compete for the same location. The repulsion between the two gives the molecule an, overall, higher energy state.

However, when the nitrogen is anti to the cholorine atom, and the methyl groups are near that hydrogen, there is no such interference. It is difficult to conceptualize the three dimensional geometry when looking at a flat structure, but Figure 2.3 attempts to display this geometry. Here, it can be seen that although the aromatic backbone requires all of the pentene ring to be flat with the left hydrogen, the two methyl groups attached to the pentene ring respectively rise above and below this plane. These methyl groups are fixed by the rigidity of the pentene ring, and, as such, the hydrogens protruding from *them* do not ever interact with the original hydrogen.

Therefore, the calculated energy differences between IR-806's three conformations make sense. The SS conformation is twice as high in energy as the AA conformation because the syn steric hindrance occurs twice. The energy difference of 7.1 KJ/mole between the AA and AS conformations results in a population ratio between the two of around 100:1 at room temperature. Likewise, there is a population ratio of 100:1 between the AS and the

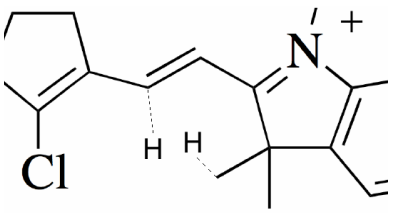

Figure 2.3: A close-up of IR-806 in anti orientation, showing how there is no longer steric hindrance when the *methyl* groups are next to the hydrogen, as opposed to the nitrogen atom.

SS conformations. This means that there is a population ratio of nearly 10,000:1 between the Aa and SS conformations. Thus, around 99% of all IR-806 molecules exist in the AA conformation. Moreover, it is hypothesized that IR-806 molecules either settle into a uniform conformation in aggregation or create an organized pattern of conformations. Aggregation depends on uniformity, and stacking would benefit from a repeated pattern of molecular alignment, and it makes sense to infer that all IR-806 molecules conform to the AA conformation for aggregation processes. Therefore, IR-806's structure is taken to be the AA conformation (as shown in Figure 2.1(b)), with the understanding that about 1% of the population could exist in the AS conformation, probably in monomer form.

While the energy minimization results confidently depict the AA conformation as by far the most stable IR-806 molecular structure, it is important to recognize the approximations and potential shortcomings of such a computational investigation. Gaussian, as a program, is limited in its capacity to realistically include solvent effects in molecular energy calculations. The solvent is treated as a continuous dielectric, so individual molecular interactions cannot be properly depicted. IR-806 most definitely interacts with water when it is in solution, as it is an anion itself, with sodium as its counter ion. IR-806 energy minimizations were performed treating molecular energies as they would appear if IR-806 were in a gas phase, and thus potential solvent interactions were completely ignored.

Moreover, the theoretical simulations could provide no information regarding IR-806 aggregation, because the addition of a second molecule would have created too many additional degrees of freedom, with many more electrons and corresponding basis functions, in the numerical approximation. There are also reasons to suggest that water itself, as a solvent, could be involved in aggregate structures.

With all of these caveats, it is important to focus not so much on the exact conformation energies or population ratios, but rather on the trend itself. The additional factors of solvent effects and molecular stacking would most likely produce minor changes to the above results, but the electron density repulsions that create steric hindrance should be the dominant cause for the differences in conformational stability. Therefore, there are still strong reasons to believe the most stable conformation for IR-806 is its AA structure, and that this conformation exists nearly on its own at room temperature.

2.2 Absorption Theory

The molecular vibrations and electronic transitions of molecules create absorption spectra, unique for each type of material. While the exact nature of the matter-light interaction is very complicated and differs dramatically depending on the situation, all interactions can be modeled by considering an electron on a spring. We choose to represent these vibrational and electronic transitions with an oscillating electron because electrons are the photon receivers in material that allow for energy excitations and transitions to occur. Mathematically, the force that the electron feels, bound to its stable state in the molecule, is represented by

$$F_{\text{binding}} = -k_{\text{spring}}x = -m\omega_0^2 x, \tag{2.1}$$

where F is the binding force, k is the spring constant of the system, x is the electron's displacement from its equilibrium position, m is the electron's mass, and ω_0 is the resonant frequency that the electron naturally oscillates at within the molecule.

The electron has an equilibrium energy state within the molecule and the oscillating electric field of the incoming light drives the electron around this equilibrium position like a driven harmonic oscillator. Mathematically, this driving force is represented by

$$F_{\text{driving}} = qE = qE_0\cos(\omega t), \tag{2.2}$$

where q is the electron's charge, E_0 is the peak electric field of the incoming radiation, and ω is the radiation frequency, in radians per second.

However, there is also damping in this situation, because the surrounding medium creates resistance to this motion. Realistically, this damping is the presence of the other particles around the electron in the molecule and surrounding matter. In this analogy with the electron, we consider radiation damping as caused by the electron's emission of radiation as it accelerates through its displacement oscillations. The simplest representation for this damping force arises by considering a force proportional to but opposing the velocity, similar to air drag. Here,

$$F_{\text{damping}} = -m\gamma\dot{x}, \tag{2.3}$$

where γ is the drag coefficient, a factor that quantifies the amount of resistance to motion contributed by the surrounding environment. It is assumed to be a constant over all of space. Putting all three of these forces together with the observed acceleration of the electron in its harmonic motion, the general equation of motion for the system is

$$F_{\text{net}} = m\ddot{x} = F_{\text{binding}} + F_{\text{driving}} + F_{\text{damping}} = -m\omega_0^2 x + qE_0\cos(\omega t) - m\gamma\dot{x}. \tag{2.4}$$

The mathematics is easier to manipulate when this equation is thought of as the real part of a larger complex equation. Then, the driving frequency that the steady state system oscillates at can be represented by a complex exponential. From here, the dipole moment of the electron can be calculated in terms of the damping coefficient, the electromagnetic driving frequency, and the resonant frequency of the system. This dipole moment can then

be used to calculate the new wave vector for the light through the material, which gives rise to the concept of light absorption. Different frequencies of light transmit with different intensities through a given material. Light that does not transmit through the material is either scattered or absorbed into the material.

If we consider the scattered light intensity negligible (which is often the case with small particles at a resonance frequency), we can look at transmitted light versus absorbed light. The damping coefficient in the equation is responsible for the absorption of energy, which must come from the energy in the electromagnetic radiation propagating through the material. The electric field drops off in exponential decay fashion as

$$E = E_0 e^{-\kappa z}, \tag{2.5}$$

where E_0 is the experimentally determined electric field at z =0 and κ is the attenuation constant, which uniquely defines the absorption properties of the material.

Practically, it is easiest to measure the intensity of this electric field, which depends on the square of the electric field amplitude. As such,

$$I = I_0 e^{-2\kappa z} = I_0 e^{-\alpha z}, \tag{2.6}$$

where I_0 is the intensity at z =0 and α, the absorption coefficient, is defined as 2κ.

In this schematic of electrons on a spring, the absorption coefficient depends on the number of the molecules per unit volume (N), resonant frequency (ω_0), electron charge (q) and mass (m), electromagnetic driving frequency (ω), damping coefficient (γ), and number of electrons with this particular resonant frequency (f) whereby

$$\alpha = \frac{Nq^2\omega^2}{m\epsilon_0 c} \sum_j \frac{f_j \gamma_j}{(\omega_j^2 - \omega^2)^2 + \gamma_j^2, \omega^2}, \tag{2.7}$$

where the constants $c = 3 * 10^8$ m/s^2 and $\epsilon_0 = 8.85 * 10^{-12}$ s^{4}A^2/m^{3}kg are, respectively, the speed of light and the permittivity of free space. The summation accounts for the fact that different electrons can resonate at different frequencies and the resultant absorption spectra combines all absorption coefficients for a range of wavelengths. When driving the electrons at their resonance frequency, there is maximum absorption. The shape of the absorption coefficient as a function of wavelength in this region is a Lorentzian curve, with maximum and FWHM unique to the material. [18]

At this point in the derivation, α appears to be an absorbance property dependent only on the type of absorbing material under consideration. However, it can be shown that α *also* depends on the density (or concentration) of the oscillators in the material. Let us define a concentration-*independent* type of absorbance coefficient, a. To start, Equation 2.6 can be written in differential form, where

$$\alpha = -\frac{1}{I}\frac{dI}{dz}. \tag{2.8}$$

The quantity $\frac{dI}{I}$ has the physical significance of being the change in absorbance intensity, as a fraction of the total absorbance intensity, whereby

$$\frac{dI}{I} = \frac{NC_{\text{abs}}}{A}, \tag{2.9}$$

where N is the total number of molecules, A is the cross-sectional area of the "slab" under consideration, and C_{abs}, the absorbance cross-section, is the fraction of absorbance that will occur for a given surface area of radiation incidence. C_{abs} *is* concentration independent, and closer to the definition of absorbance coefficient that we are looking for. We are almost there.

Substituting back into Equations 2.8 and 2.9, we can write,

$$dz = \frac{NC_{\text{abs}}}{A}, \tag{2.10}$$

which can be rewritten with the use of Equation 2.8 (and the simplification that at this point $dz = z$), as

$$\alpha = \frac{NC_{\text{abs}}}{V} = c_{\text{N}}C_{\text{abs}} = c_{\text{M}}N_AC_{\text{abs}}, \tag{2.11}$$

where V is the volume of the entire material sample, c_{N} is the number concentration of molecules, c_{M} is the molar concentration of molecules, and $N_A = 6.022 * 10^{-}23$ particles/ mole is Avogadro's number.

This last conversion into concentration units of molarity is for convention. Also, the spectrophotometers that chemists use output readings of absorbance as the log base 10 of the intensity ratio. As such, an additional factor of $2.3 = \ln(10)$ must be accounted for. With all of these considerations, we can finally define the total absorbance (A) as

$$A = \frac{\alpha z}{2.3} = \frac{c_{\text{M}}N_AC_{\text{abs}}z}{2.3}. \tag{2.12}$$

Now, we can define an absorption property, independent of sample thickness and concentration, that absorbs the constants N_A and 2.3, such that

group N_A and 2.3, as constants, with C_{abs} to define our absorbance quantity of interest (a), where

$$A = aC_{\text{abs}}z. \tag{2.13}$$

At last, we have *our* definition for the absorbance coefficient (a).

$$a = \frac{A}{C_{\text{abs}}z} = \frac{N_AC_{\text{abs}}}{2.3}. \tag{2.14}$$

In materials that do not aggregate or have concentration dependent molecular properties, a remains constant with concentration. However, in the case of chromonic liquid crystals, where aggregation occurs at low concentration and fundamental molecular properties change with concentration, a is no longer fixed. Moreover, referring back to Equation 2.7, it is evident that a given material may have multiple resonant frequencies that correspond to different wavelengths of light. Observations of how a chromonic's entire absorption coefficient spectrum changes with concentration provides strong insight into the relevant aggregation mechanisms at play.

2.3 Aggregation Theory

Chromonic liquid crystal aggregation can be explored from the perspective of a chemical reaction mechanism with equilibrium constants that describe the completion of the various reactions at play.

In general, the equilibrium constant describes the completeness of a chemical reaction's conversion of reactant to products. For example, let us consider the chemical reaction

$$aA + bB \rightleftharpoons cC + dD, \tag{2.15}$$

where A and B are reactants interacting to yield products C and D, and their stoiciometric coefficients are respectively given by a, b, c, and d. The reaction's equilibrium constant is given by

$$K_{eq} = \frac{[C]^c[D]^d}{[A]^a[B]^b}, \tag{2.16}$$

where brackets denote molecular molar concentrations (moles solute/ liters solution) after the system has relaxed to stable equilibrium.

In the case of molecular self-association, as is the case with chromonic aggregate formation, reactions are assumed to take place by additions of single monomers to either other monomers or n-mers. As such, aggregation occurs through monomer addition, and the notion of a stacking free energy change is preserved.

For a given total dye concentration, the relative amounts of aggregate species can be determined by combining all possible reactions taking place together in solution. Let A be the monomer species and A_n signify the n-mer species consisting of n monomers. Each reaction involving addition of a monomer to each n-mer could, theoretically, have its own equilibrium constant that determines the drive for aggregate formation. Such a reaction is represented by

$$A_{n-1} + A \rightleftharpoons A_n;\ K_n = \frac{[A_n]}{[A_{n-1}][A]}. \tag{2.17}$$

To quantify the equilibrium constant associated with such a reaction, however, it is necessary to describe $[A_{n-1}]$ in terms of $[A]$ and the total dye concentration, C_T. It is also helpful to refer to the molar concentration of each species in terms of its dye weight fraction, α_n, where

$$\alpha_n = n[A_n]/C_T. \tag{2.18}$$

Therefore, let us begin such a derivation. The mechanism for dimer formation is straightforward, whereby

$$2A \rightleftharpoons A_2;\ K_2 = \frac{[A_2]}{[A]^2}. \tag{2.19}$$

Likewise, trimer formation consists of

$$A_2 + A \rightleftharpoons A_3;\ K_3 = \frac{[A_3]}{[A_2][A]}, \tag{2.20}$$

where Equation 2.19 can be used to substitute $K_2[A]^2$ for $[A_2]$. In similar fashion, the equilibrium constant for a tetramer can either be written in terms of $[A_4]$, $[A_3]$, and $[A]$ or by substituting $K_2K_3[A]^4$ in for $[A_3]$.

Through consideration of consecutive reactions in aggregate formation, a pattern surfaces that allows us to define $[A_n]$ in terms of $[A]$ and previous equilibrium constants. In all,

$$[A_n] = (K_2...K_{n-1})[A]^n. \tag{2.21}$$

While these equations are useful in the sense that properly depict relationships between the factors at play, they are not realistically helpful because we generally have no means for experimentally deriving molar concentrations for each aggregate species in solution. We can only control the total molar concentration, where

$$\begin{aligned} C_T &= [A] + 2[A_2] + 3[A_3] + ... + n[A_n] \\ &= [A]\left(1 + 2K_2[A] + 3K_2K_3[A]^2 + ... + n(K_2...K_n)[A]^n\right), \end{aligned} \tag{2.22}$$

where n represents the number corresponding to the largest n-mer in solution.

From here, aggregate species mole fractions can be defined, where mole fraction, analogous to weight fraction in this situation, is the moles of dye in a particular aggregate specie in solution, relative to the total number of moles of dye in solution. Because all concentration units have been discussed in terms of molarity, simply dividing molar concentrations will yield a fraction comparing moles alone. For example, the monomer mole fraction, denoted as α, is expressed as

$$\alpha = \frac{[A]}{C_T} = (1 + 2K_2[A] + 3K_2K_3[A]^2 + ... + n(K_2...K_n)[A]^n)^{-1} + ... \tag{2.23}$$

Molar fractions for all other aggregate species can similarly be calculated using Equation 2.23 with 2.21.

Through these calculations, it has been shown that relevant quantities explaining aggregation self-assembly can be expressed in terms of α and relevant equilibrium constants [19]. However, difficulty arises in actually quantifying such mechanisms when each reaction has a different equilibrium constant. The general case, therefore, is frequently recast in more constrained terms, whereby either all equilibrium constants are taken to be equal or only K_2 is allowed to differ from all other equilibrium constants. The first case is the mechanism for the previously mentioned isodesmic aggregation, and the second accounts for environments where the dimer is either more energetically favorable than higher order aggregates or is less favorable, and a critical concentration must be reached (similar to a critical micelle concentration) before dimerization can occur. After this concentration threshold is crossed, further aggregation rapidly ensues.

In isodesmic aggregation, also called the Equal K (EK) Model, all equilibrium constants are denoted by K_E, and, as such, no distinction is made between the various K_n previously discussed. This simplifies the mathematics considerably, for now

$$C_T = [A](1 + 2K_E[A] + 3(K_E[A])^2 + ... + (n+1)(K_E[A])^n + ...). \tag{2.24}$$

If two additional terms are introduced, $x = K_E[A]$ and $L = K_E C_T$, then substitution of these parameters into Equation 2.24 yields

$$L = x(1 + 2x + 3x^2 + ... + (n+1)x^n + ...) = \frac{x}{(1-x)^2}, \tag{2.25}$$

through the use of a Taylor expansion, with the constraint that x is always less than one. There are two solutions to Equation 2.25, only one of which allows for x less than one. This solution is

$$x = \frac{2L + 1 - \sqrt{4L+1}}{2L}. \tag{2.26}$$

which, by substituting in $\alpha = [A]/C_T = x/L$ transforms Equation 2.23 into

$$\alpha = \frac{2L + 1 - \sqrt{4L+1}}{2L^2}. \tag{2.27}$$

Now, the entire mechanism can be described by just the two parameters K_E and C_T. Relative concentrations and weight fractions of monomer and any n-mer can be determined from combining Equation 2.27 with Equation 2.23. Figure 2.4 shows theoretical mole fractions for isodesmic aggregation between dye concentrations of 0.1-10 mM, where K_E is 500 M^{-1}.

Realistically, however, initial aggregation of monomers into dimers is frequently controlled by a different equilibrium constant, one that makes dimer formation either more favorable than larger aggregates, or hinders dimer formation such that a critical monomer concentration is required before it becomes thermodynamically favorable to begin the aggregation process. Both of these cases can be accounted for by allowing K_2 to differ from all other equilibrium constants, such that

$$K_2 = \rho K_E, \tag{2.28}$$

and K_E remains the universal equilibrium constant to describe all K's other than K_2. The constant of proportionality, ρ determines whether dimer formation is more favorable or less favorable than all other reactions involved in the aggregation mechanism. If ρ is greater than one, then the mechanism is called "dimer enhanced," and if ρ is less than one, then the mechanism is analogous to an "unfavorable endcaps" scenario. When an aggregate stack has "unfavorable endcaps," its molecules are less stable when bound to the end of a stack, as opposed to somewhere in the interior. Thus, dimerization is the most thermodynamically hindered process. When dimers finally begin to form in solution, larger aggregates readily form. Also, such a process is conceptually similar to a special type of cooperative mechanism, whereby a critical concentration of monomers is required in order to begin dimerization.

Frequently, a cooperative mechanism corresponds to the presence of a nucleation process, where a monomer must change into an unstable form in order to form a dimer. This unstable conformation can be an infrequent occurrence, which makes dimer formation the limiting factor in the aggregation process [20]. Generally, dimer enhanced mechanisms occur among neutral molecules with more steric hindrance.

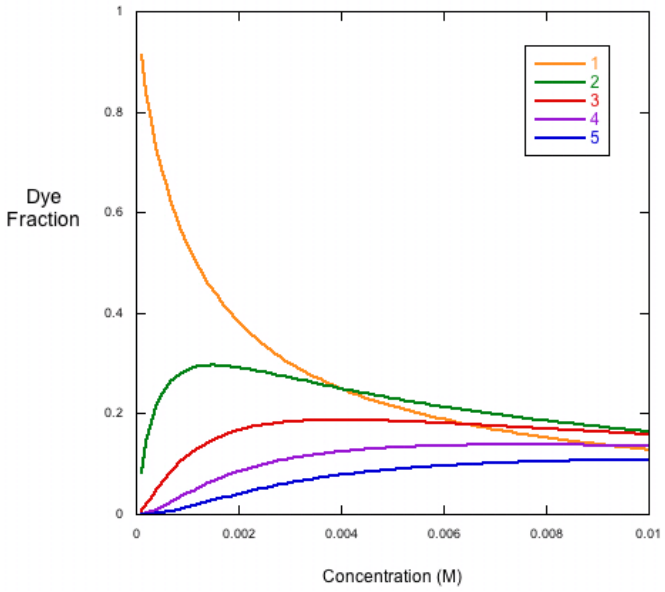

Figure 2.4: Example of molar fractions for different species in Isodesmic Aggregation where the universal equilibrium constant is 500 M^{-1}. Each curve is color coded to connect with its respective n-mer.

The Unequal K theory is more complicated than the Equal K model, but still allows for analytical solubility. Choice of dimer uniqueness in Equation 2.28 changes Equation 2.22 into

$$C_T = [A]\left(1 + \rho(2K_E[A] + 3(K_E[A)]^2 + ... + (n+1)(K_E[A])^n) + ...\right) \tag{2.29}$$

and changes Equation 2.25 such that

$$L = x\left(1 + \rho(2x + 3x^2 + ... + nx^n + ...)\right) = x(1-\rho) + \frac{\rho x}{(1-x)^2}, \tag{2.30}$$

where the same Taylor expansion is used from Equation 2.25, except now the incorporation of ρ beginning at the second term of series requires subtracting off $x\rho$ from the initial x term. Equation 2.30 can also be rewritten to define α. The relation $\alpha = x/L$ still holds, and, as such

$$\alpha = \frac{1}{(1-\rho) + \frac{\rho}{(1-x)^2}} = \frac{(1-x)^2}{1 - x(2-x)(1-\rho)}. \tag{2.31}$$

It is important to note that Equation 2.31 reduces to the Equal K analogy of Equation 2.27 in the limit that ρ equals one. All this excess derivation is just a special case where the dimer equilibrium constant is different than the other equilibrium constants.

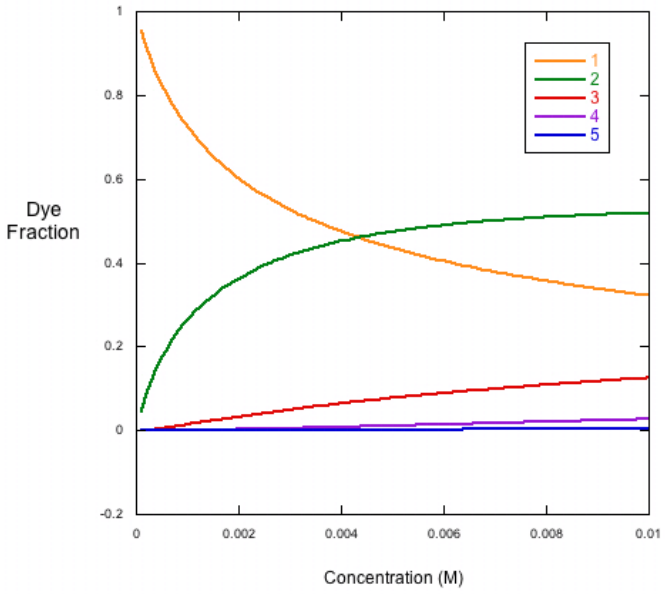

Figure 2.5: Various dye fractions vs. concentration for different species in an example of Dimer Enhanced Aggregation, where the universal equilibrium constant is 5000 M^{-1}, and ρ is 5 (making the dimer equilibrium constant 25,000 M^{-1}). Each curve is color coded to connect with its respective n-mer. The total dye concentration range spans the same concentrations as shown in the Isodesmic example of Figure 2.4, ranging between 0.1 and 10 mM. Note how the population of dimers continues to increase at high concentrations, in contrast to the Isodesmic example.

While Equation 2.27 is quadratic in α, Equation 2.31 is cubic. We can then use the relation $x = \alpha L$ to obtain

$$0 = \alpha^3 L^2(\rho - 1) + \alpha^2 L(L - 2(\rho - 1) - \alpha(2L + 1) + 1. \tag{2.32}$$

This is the final cubic equation from which one solution provides the final quantification of α in terms of L. Once this equation is solved, all components of the process can be explained in terms of C_T, K_E, and ρ. After α is defined in this way, so too can the other aggregate weight fractions. In this situation,

$$\alpha_n = \frac{\rho n[A]^n K_E^{n-1}}{C_T} = n\rho\alpha x^{n-1} = n\rho\alpha^n L^{n-1}, \tag{2.33}$$

where in this formula n is constrained to being an integer greater than one.

With three parameters that can vary, best fit equations can be applied to real data to determine whether an isodesmic or cooperative theory best supports experimental results. Figure 2.5 shows an example of various aggregate species' mole fractions in an Unequal K

model, where dimerization is enhanced. The same concentration range is used here as was for Figure 2.4.

In the example demonstrated by Figure 2.5, it is evident that aggregation occurs at a much lower concentration than in Figure 2.4. This is because the equilibrium constant for the first step in the reaction is considerably larger for the dimer enhanced model than for isodesmic aggregation, given the same concentration range and general equilibrium constant. The substantial number of dimers produced at lower concentration spurs the formation of higher aggregate structures. Therefore, aggregation as a whole is aided.

However, the unequal K model supports an entirely different type of aggregation, mentioned earlier as having a mechanism that requires a critical concentration for dimerization. This situation occurs when $\rho < 1$ and the dimer equilibrium constant is actually smaller than all other equilibrium constants for larger aggregates in the mechanism. Figure 2.6 shows an example of dye fraction for various n-mers in a situation where ρ is less than 0.05. Note that a larger general equilibrium constant is needed to overcome the unfavorable nature of the dimerization reaction.

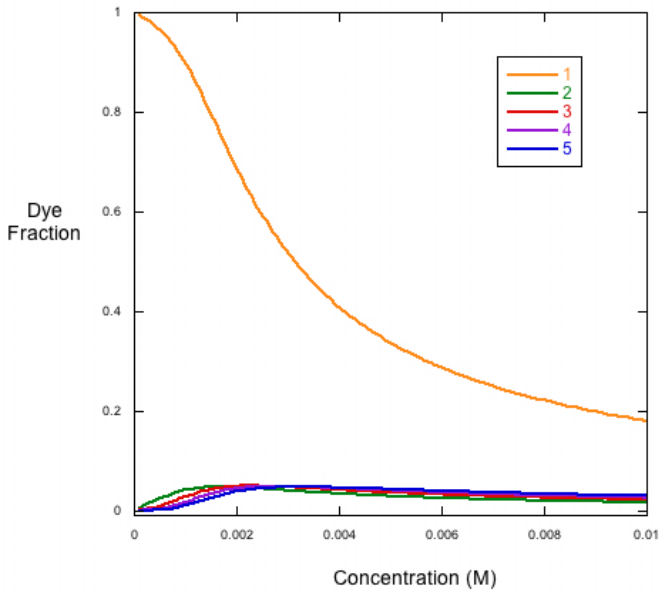

Figure 2.6: Example of various dye fractions for different species in "Unfavorable Endcaps" Aggregation, where the universal equilibrium constant is 500 M^{-1}, and ρ is 0.01 (making the dimer equilibrium constant 5 M^{-1}). Each curve is color coded to connect with its respective n-mer. The total dye concentration range spans a concentration range from 0.1-10 mM. The dimer concentration in solution is always minimal, and it decreases at higher concentrations like the dimer concentration in Isodesmic Aggregation.

This model is analogous to an aggregate having "unfavorable endcaps," where having exposed ends in the aggregate structure is energetically unfavorable. Physically, such properties case arise in rigid ringed structures where aggregation forces the backbone to bend in a slightly unfavorable way. If the conjugated backbone of a chromonic has *two* molecules bonded to it (one above and one below), then the bending compensated by the extra π bonding. In this case, dimers are the *least* energetically favorable aggregate in solution, so it will take a much larger monomer concentration to create a strong enough driving for their formation. Then, as soon as the dimers are formed, they will aggregate into larger stacks. [21]

2.4 Birefringent Optics

While light travels at the fundamental speed of $3*10^8$ m/s in a vacuum, its rate of propagation instantly slows to a new constant when it reaches a material interface. The exact speed depends on the molecular structure comprising the matter, and the proportionality constant relating the speed of light through a material to that of a vacuum is defined to be a material's refractive index,

$$n = \frac{c}{v}, \tag{2.34}$$

where v is the speed of light through the material and n is the refractive index. Light propagation is very sensitive to molecular differences, and refractive index tests can identify and distinguish between compounds whose chemical structures differ by only an atom. Indeed, the *CRC Handbook for Chemistry and Physics* contains a refractive index for most known liquids at 20 °C accurate to the fifth decimal place.

Liquids and other isotropic media have a single refractive index depending on their temperature, but anisotropic materials have multiple refractive indices because molecular composition depends on direction within the sample. Frequently one refractive index is responsible for light interaction along the axis parallel to the direction of molecular alignment, and a second refractive index along an axis perpendicular to the direction of molecular alignment. Light slows down when it travels through a material, not because matter physically impedes its progress forward, but, rather, because the electric field of the radiation interacts with the parallel component of the material's polarizability. Thus, the orientation of the light's electric field, or polarization, determines the speed at which light travels through the material. If light is linearly polarized along a particular axis by an angle θ from the axis of molecular alignment, then the parallel and perpendicular components of the light's electric field will induce differing amounts of polarization into their surrounding media and propagate at different rates.

Let us represent this linearly polarized electromagnetic radiation as wave propagating along the z-axis. Denoted by

$$\psi(z,t) = A\cos(kz - \omega t + \delta), \tag{2.35}$$

ψ is the wave equation, A is the peak amplitude, $k = \frac{2\pi}{\lambda}$ is the angular wavenumber, z is the displacement, ω is the angular frequency, t is elapsed time, and δ is the phase offset of

the wave relative to another wave. The generated electric field, oscillating in the xy plane, can be separated into components respectively parallel and perpendicular to the material's molecular alignment,

$$\vec{E} = \vec{E_{\shortparallel}} + \vec{E_{\perp}}. \tag{2.36}$$

Since these electric field components are created by separate spatial components within the electromagnetic wave vector,

$$E_{\shortparallel} = \vec{E}\cos(k_{\shortparallel}z - \omega t + \delta_{\shortparallel}) \text{ and } \vec{E_{\perp}} = \mathbf{E}\cos(\mathbf{k}_{\perp}\mathbf{z} - \omega\mathbf{t} + \delta_{\perp}), \tag{2.37}$$

and we can treat the overall wave vector of Equation 2.35 as a superposition of two wave vectors, with the parallel and perpendicular components, respectively.

As these two wave components are decoupled, we can separately analyze their retardation through some anisotropic material. Initially, (as the incoming light has been linearly polarized) both waves are exactly in phase, so $\delta = 0$. However, when the parallel wave enters the medium its speed is reduced by a factor of $n_{\shortparallel}$, which is mathematically expressed as an increase in its wave vector by a factor of $n_{\shortparallel}$. The perpendicular wave similarly transforms, except that its speed is reduced by a factor of $n_{\perp}$, depicted as an increase of its wave vector by $n_{\perp}$.

As such, after a total distance d is travelled by both the parallel and perpendicular electromagnetic wave components, the argument in $E_{\shortparallel}$ has increased by $n_{\shortparallel}k_0d$ while the argument in $E_{\perp}$ has increased by $n_{\perp}k_0d$. Thus, the difference in their two arguments, δ is quantified by

$$\delta = (n_{\shortparallel} - n_{\perp})k_0d = \frac{2\pi d(n_{\shortparallel} - n_{\perp})}{\lambda_0} \tag{2.38}$$

From here, the birefringence is defined as [3]

$$\Delta n = n_{\shortparallel} - n_{\perp} = \frac{\delta\lambda_0}{2\pi d} \tag{2.39}$$

A material with such birefringence is also known as a phase retarder, because it changes the relative phases between polarized light parallel and perpendicular to the direction of the material's alignment. In order to quantify and track the relative polarization of light through and optical system, we shall use Jones' Matrices.

2.5 Jones' Vectors and Matrices

The use of Equation 2.39 allows us to calculate the birefringence of a medium given the phase difference between the arguments of two electric field components. In reality, experimental determination of birefringence relies on observing an intensity change in the electric field after it has gone through a birefringent medium. Let us set up the situation previously discussed, where linearly polarized light passes through an optical system consisting of two perpendicularly oriented polarizers "sandwiching" a chromonic sample in its liquid crystal

phase. Let us also set the first polarizer to be aligned with the incoming horizontally polarized light.

Given that light propagation is along the z axis, the direction of polarization is somewhere on the xy plane. Thus, it can always be broken up into its x and y components into a two dimensional column vector. In the most general case, light polarization is represented as

$$\mathbf{E} = \begin{bmatrix} E_{x_0} e^{i\phi_1} \\ E_{y_0} e^{i\phi_2} \end{bmatrix} e^{i(kz-\omega t)}. \tag{2.40}$$

It is important to note that we are only interested in the *difference* between x and y components of polarization. Therefore, while the vector may be needed to be multiplied by other factors to depict the total electric field of wave, these other factors do not need to be included in assessing the birefringence of our material. Ultimately, all multiplicative factors will be lumped together and obtained through *experimental fitting*. As such, it is common practice and actually much easier to pull out common factors between the x and y polarizations and then neglect those factors thereafter.

Because we are only interested in the relative polarization between the x and y axes , we begin to asses our optical system *after* the laser light has passed through the first polarizer. We can set our x axis to align with this polarizer's direction of polarization, so the initial polarization of our incident light upon the liquid crystal sample can be portrayed as

$$\mathbf{E} = \begin{bmatrix} 1 \\ 0 \end{bmatrix}. \tag{2.41}$$

Now, let us represent the liquid crystal sample, acting as phase retarder, with Jones matrix form of

$$\mathbf{R}_H = \begin{bmatrix} e^{i\phi_x} & 0 \\ 0 & e^{i\phi_y} \end{bmatrix}, \tag{2.42}$$

where ϕ_x and ϕ_y are respectively the phase changes added to the x and y directions of polarization after propagation through the material.

However, since we are only interested in the relative phase difference between the two dimensions, we can factor out ϕ_x from the matrix, subsume the multiplicative factor, and obtain

$$\mathbf{R}_H = \begin{bmatrix} 1 & 0 \\ 0 & e^{i\delta} \end{bmatrix}, \tag{2.43}$$

where δ is the same phase shift defined in Equation 2.38. To do this, we must align the phase retarder such that the x axis is parallel to aggregate alignment, fixing the y direction perpendicular to it.

To generalize this equation to allow for any angled orientation of a phase retarder, we apply rotation matrices onto the horizontally oriented phase retarder operator, where any

general two dimensional rotation matrix can be represented by

$$\mathbf{\Theta}_\theta = \begin{bmatrix} \cos\theta & -\sin\theta \\ \sin\theta & \cos\theta \end{bmatrix}. \tag{2.44}$$

In our application of the rotation matrices on a general phase retarder oriented at angle θ, we first operate on the retarder with an inverse rotation matrix (equivalent to rotation by angle $-\theta$), so that the retarder can be brought "back" to alignment with the horizontal axis. Then, we apply the counterclockwise rotation of same angle to bring the retarder back into its initial orientation. The result is as follows:

$$\mathbf{\Theta}_{-\theta}\mathbf{R}_H\mathbf{\Theta}_\theta = \begin{bmatrix} \cos\theta & \sin\theta \\ -\sin\theta & \cos\theta \end{bmatrix} \begin{bmatrix} 1 & 0 \\ 0 & e^{i\delta} \end{bmatrix} \begin{bmatrix} \cos\theta & -\sin\theta \\ \sin\theta & \cos\theta. \end{bmatrix}$$

Simplifying this expression yields

$$\mathbf{R}_\theta = \begin{bmatrix} \cos^2\theta + e^{i\delta}\sin^2\theta & \sin\theta\cos\theta(e^{i\delta}-1) \\ \sin\theta\cos\theta(e^{i\delta}-1) & e^{i\delta}\cos^2\theta + \sin^2\theta \end{bmatrix}, \tag{2.45}$$

and we now have the general form for a phase retarding operation. Another way to conceptualize this multi-step transformation is to leave the phase retarder fixed in its angle θ orientation and rotate the light polarization instead. Given the light is initially horizontally polarized, if we apply a rotation transformation to align the light polarization with the retarder, then the retarder will act just as in the specific case mentioned before. After we have treated the special case, we can then apply the inverse rotational transformation to bring the light polarization back to its initial horizontal polarization. Either way, the rotation matrix and its inverse allow us to shift frames and use the convenient special case to derive the general one.

To evaluate the resultant light polarization through our phase retarder system, all components of the system must operate, in order, on the incoming light. We again consider our light as initially horizontally polarized, as it is standard for each experiment. Therefore, evaluating the incoming light (through the horizontal polarizer), phase retarder, and vertical (crossed) polarizer, the resultant light polarization is determined by

$$\mathbf{P}_V\mathbf{R}_\theta\mathbf{E}_H = \begin{bmatrix} 0 & 0 \\ 0 & 1 \end{bmatrix} \begin{bmatrix} \cos^2\theta + e^{i\delta}\sin^2\theta & \sin\theta\cos\theta(e^{i\delta}-1) \\ \sin\theta\cos\theta(e^{i\delta}-1) & e^{i\delta}\cos^2\theta + \sin^2\theta \end{bmatrix} \begin{bmatrix} 1 \\ 0 \end{bmatrix}. \tag{2.46}$$

Therefore, evaluating each component of the optical system, the resultant relative difference in light polarization is determined by

$$\mathbf{E}_{\theta,\delta} = \begin{bmatrix} \sin\theta\cos\theta(e^{i\delta}-1) \\ 0 \end{bmatrix} \tag{2.47}$$

To obtain a final light intensity dependent on both the phase retarder angle orientation and relative phase shift, we take the modulus squared of our complex vector and obtain

$$I_{\theta,\delta} = \begin{bmatrix} \sin\theta\cos\theta(e^{-i\delta}-1) & 0 \end{bmatrix} \begin{bmatrix} \sin\theta\cos\theta(e^{i\delta}-1) \\ 0 \end{bmatrix} = \sin^2\left(\frac{\delta}{2}\right)\sin^2(2\theta). \tag{2.48}$$

In all, these calculations quantify how a phase retarder turns linearly polarized light into elliptically polarized light. Linearly polarized light has no phase difference between the x and y components of its polarization. However, when linearly polarized light travels through a birefringent material, the x and y components of polarization experience different environments and a phase difference develops between them. This phase change depends on properties intrinsic to the phase retarding material, and the total amount of light that gets through the crossed polarizers (as elliptically polarized light) depends on both this phase change and the relative angle between the phase retarder and the crossed polarizers.

With this information, one can see that, for a given δ, the light intensity through the crossed polarizers is maximized when θ is 45°. Realistically, there is no way to know at first glance how the liquid sample is oriented relative to the crossed polarizers, but one can experimentally find this angle by rotating the sample until the detected light intensity is maximized. Also, the thickness of the sample can be varied, such that $\sin^2\left(\frac{\delta}{2}\right)$ is not too small.

Chapter 3

Experimental Methods

3.1 Degradation

Previous research involving IR-806 noticed that bleaching had occurred over time with solutions in both water and methanol. It was noted that the water solutions degraded more quickly than the solutions in methanol. [11] Given that this research involves water-based solutions of IR-806 over a variety of concentration ranges, it was important to assess the possibility for solution degradation and, in the case that it was observed, attempt to quantify its causes and avoid those environments as much as possible.

IR-806 degradation was quantified by measuring how its absorption coefficient changed over a span of time. The term "bleaching" refers to a general decrease in overall coloring, but an exact comparison of absorption spectra over time would provide quantitative data regarding how quickly absorption decreases over time and the spectrum's shape changes in addition to generally decreasing. If the absorption coefficient changes, then fundamental molecular properties change as well. Either the structure of the individual molecule has changed, or the aggregate structure has been altered.

An initial degradation test was done to see if degradation depended on how much light the sample was exposed to. Two containers of low concentration IR-806 solution were respectively kept in light and dark environments, and spectrophotometer readings were taken daily for about two weeks. The absorbance coefficient at the 800nm peak versus time provided a means for comparing the rates of absorbance decay. While the "dark" solution degraded more slowly than the "light" solution, both solutions decayed at similar rates. There was not enough evidence to confidently label light as the primary cause for IR-806 solution degradation.

Informal degradation was also observed for more concentrated IR-806 solutions. It was noted that the higher concentration solutions retained their color and spectral properties for a longer time than the lower concentration solutions. Therefore, further experimentation was limited to low concentration samples, in order to understand the worst case scenario. Furthermore, it was hypothesized that a low concentration of 0.0005 wt% IR-806 would contain mostly monomers in solution. The presence of absorption degradation without aggregates

would mean that the molecular structure of IR-806 was unstable in solution. This is an important finding because all further aggregation and liquid crystal properties depend on the stability of the individual molecule.

In a second test, an experiment was performed that tested IR-806 degradation's dependence on solution acidity. 0.0005 wt% solutions of IR-806 were created in phosphate buffers of respectively pH 2.8, 7.3, and 10.5. A combination of H_3PO_4 and NaH_2PO_4 created the acid environment; a combination of NaH_2PO_4 and Na_2HPO_4 created the neutral environment, and a combination of Na_2HPO_4 and Na_3PO_4 created the basic environment. Concentrated HCl and NaOH were used to obtain the exact pH desired. Again, solution absorbance vs. time at the 800nm peak served as a comparison for degradation rate. It turned out that acidity proved to be an important factor in IR-806 stability. Namely, acidity in solution is a major cause for IR-806 solution degradation over time. These results are discussed in Chapter 4.

3.2 Phase Diagram

A phase diagram for IR-806 showing the liquid crystal region based upon temperature and concentration was constructed by a combination of two techniques. An initial idea of the phase diagram was obtained by qualitatively observing the appearance of the solution under a polarizing microscope, and a final version of the phase diagram was constructed by quantitatively measuring the transmitted light intensity through the sample when placed between crossed polarizers. Both methods used similar techniques for sample preparation. The microscope observation provided a general idea about what the phase transitions looked like, and the laser experiment generated a systematic reading of exactly where these transitions occurred.

3.2.1 Polarizing Microscope

Various concentrations between 0.5 and 2.0 wt% were created for observation under a Leitz Laborlux 12 polarizing microscope. The polarizing microscope was set up such that an initial light source traveled through the liquid crystal, which was on a rotating mount and sandwiched between polarizers that were crossed. In this way, one could observe the birefringence of the liquid crystal directly, and observe *how* the various domains were oriented relative to one another. The microscope had an attached heating and cooling system, so the appearance of the solution could be observed as it was heated and cooled. The 1.41 and 1.99 wt% solutions were observed when heated starting from room temperature, and the 0.95 and .42 wt% solutions were observed when heated starting from a variety of initial temperatures, the lowest around 13℃.

Microscope samples were prepared by pipetting the sample onto a glass microscope slide, and epoxying 25 µm by 25 µm cover slip around the edges. The sample was protected from evaporation for the duration of the immediate testing, but needed to be reproduced daily. Therefore, every experimentation used a new slide.

3.2.2 Crossed-polarizer Laser Apparatus

To examine these changes, a more accurate laser apparatus was used. The system involved a helium-neon laser emitting light of wavelength 633 nm, a chopper causing the light to pulse in a square wave of frequency of 150 Hz, two polarizers, the sample, and lock-in amplifier set to read signals with a frequency of 150 Hz. The first polarizer was placed in front of the sample holder and the second polarizer was placed after the sample holder, crossed with the first such that only light undergoing a phase shift would reach the detector. The sample holder was also connected to a heating and cooling system so that the temperature of the sample could be controlled. A schematic diagram of the apparatus is shown below in Figure 3.1.

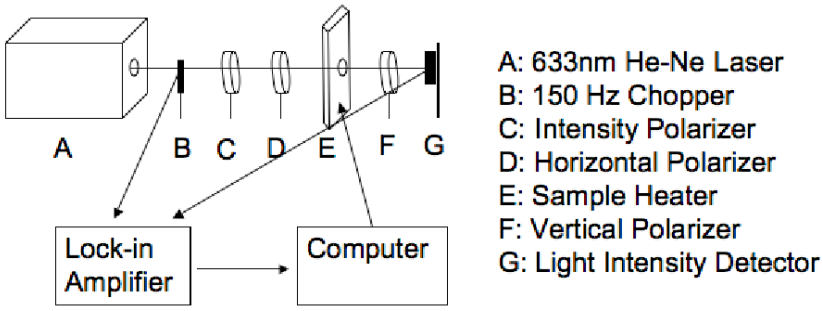

Figure 3.1: Laser Apparatus

Because a lock-in amplifier was used, experiments could be done with the room light on. By initially orienting the sample such that a maximum amount of light was reaching the detector before any heating, it could be inferred that any decrease in light intensity was due to a decrease in birefringence, rather than a re-orientation of the liquid crystal director as heating occurred. The laser experimentation used the same method of sample preparation as did the microscope, and a new slide was similarly prepared for every run. Also, a 2.48 wt% solution was tested in the laser apparatus, along with the previously used concentrations. Samples were cooled down to 15 ℃, given time to equilibrate, and then observed as they were heated at 1 degree per minute. Data were taken every 10 seconds.

3.3 Absorption Spectra

Absorption measurements of IR-806 were taken on a Jasco UV/Vis spectrophotometer in the wavelength range of 350-1100nm. Because IR-806 forms a liquid crystal phase at such a low concentration, we made our lowest concentration as dilute as possible, such that absorbance could still be observed in the spectrophotometer with a cuvet thickness of 10mm. A total of 14 concentrations were prepared, ranging from concentrations of 0.000499-0.966 wt%. Table **??** shows all 14 concentrations of IR-806 tested, with the cuvet length used for each sample. As the solution's concentration increased, the cuvet path length needed to decrease so that

the measured absorbance could remain in the region where the spectrophotometer readings were linear.

Table 3.1: Absorbance Measurements: IR-806 Concentrations and Cuvet Lengths for

Concentration (wt%)	Cuvet length (mm)
0.000499	10
0.00102	4.0
0.00500	2.0
0.0153	1.0
0.0353	0.11
0.0497	0.11
0.0668	0.11
0.101	0.11
0.110	0.11
0.249	0.0247
0.303	0.0117
0.387	0.0168
0.565	0.0163
0.966	0.0107

Because the 0.1 mm cuvet consisted of pressing two quartz slides together, exact thickness was determined through calibration with a K_2CrO_4 solution in HCl. The absorbance of the calibration solution was measured at 352.6 nm in both the quartz 1mm and 0.1mm cuvets. Given that the absorbance coefficient of the solution is constant between these two measurements and that the 1mm cuvet is accurately 1.0mm in thickness, the 0.1 mm cuvet was determined to actually have a path length of 0.11mm. This thickness was used instead of 0.1mm as the light path length for the afore mentioned IR-806 solutions ranging between concentrations of 0.0353-0.110 wt%.

IR-806 concentrations greater than 0.110 wt% required an even smaller path length for a reliable absorbance measurement, and glass slides were prepared from microscope slides, epoxy, and glass spacers for these measurements. Because the microscope slides were twice the width of the spectrophotometer sample holder, they were cut in half and the two sides could be attached by small dabs of an epoxy and glass spacer mix at each corner. In this way, the slides had a small, even gap between them, with dimensions to fit nicely in the spectrophotometer. Either 10 or 25 micron spacers were used, depending on the solution concentration.

The technique used to measure the exact thickness of the slides entailed taking the absorbance spectra of the slide alone before sample insertion. Because the glass slides were parallel to one another, observable interference peaks in the absorbance spectra served as a

means for determining the exact thickness. When treated as a thin film reflection interference situation, a plot of peak wavelength vs. interference order can be fit with the path difference as a parameter in the best fit equation. Such analysis allowed for slide thickness calculation before IR-806 absorbance measurement.

While the spectrophotometer measured absorbance vs. wavelength, all data would be converted into absorbance coefficient vs. wavelength, such that comparisons could be both path length and concentration independent.

3.4 Peak Fitting

Referring back to Equation 2.23, absorbance theory predicts that when a material absorbs at a particular electromagnetic frequency, a Lorentzian peak occurs in a plot of absorbance vs. frequency. An example normalized Lorentzian curve is shown in Figure 3.2. A Lorentzian distribution is defined by its center x value, and a parameter, γ, that determines how sharply the curve falls off for x values increasing far away from the center value.

It is important to note that, technically, absorbance theory predicts a Lorentzian distribution for one type of transition in a plot of absorbance amplitude vs. electromagnetic *frequency*. This means that a plot of absorbance vs. *wavelength* will not give exactly the same distribution, as there is an inverse relationship between electromagnetic frequency and wavelength. However, for our relatively narrow range of wavelengths, this discrepancy is small and can be neglected.

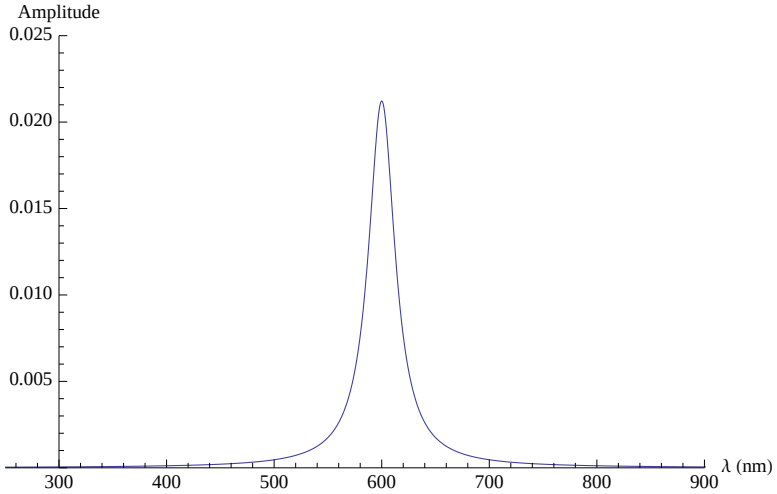

Figure 3.2: Example Lorentzian curve. The general equation for a normalized Lorentzian is: $y = \pi\gamma\left((x_0 - x)^2 + \gamma^2\right)^{1/2}$, where, in this example, $x_0 = 600$nm, and $\gamma = 15$

As can be seen in Figure 3.2, a Lorentzian distribution is very narrow at is peak, and significantly broadens at its base. In fact, the Lorentzian distributions that result from such resonance frequency transitions are too narrow to be experimentally observed in large molecules like IR-806.

Because atoms undergoing transitions are so close to other atoms in the molecule, near-neighbor effects create spectral broadening that widens the various initially Lorentizan distributions into a more Gaussian shape. When a molecule is in solution, these effects are even more pronounced, as near-neighbor effects are exacerbated by the fact that surrounding molecules in solution are can be experiencing different transitions and provide variable sources of energy to molecules through collisions. In the case of low concentrations IR-806 solutions, the absorption spectra are entirely dominated by this spectral broadening and look entirely Gaussian in shape. Figure 3.3 shows an example normalized Gaussian distribution.

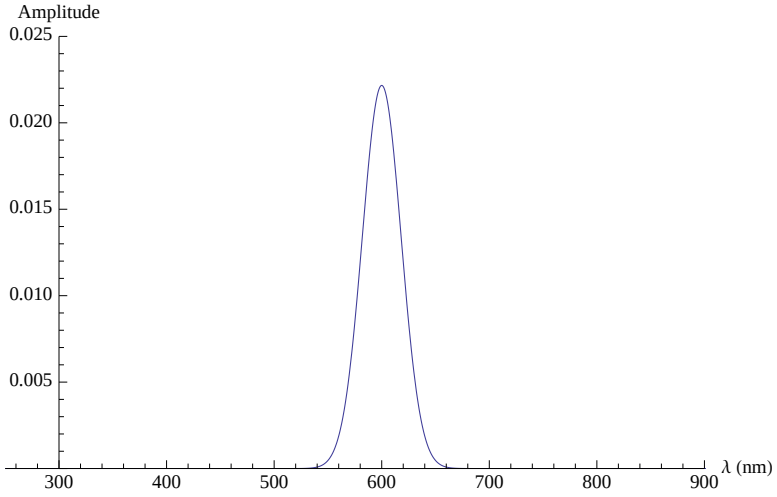

Figure 3.3: Example Gaussian distribution. The general equation for a normalized Gaussian is: $y = \frac{1}{\sigma\sqrt{2\pi}} e^{\frac{-(x-x_0)^2}{2\sigma^2}}$, where, in this example, $x_0 = 600$nm, and $\sigma = 18$ nm

For a Gaussian, x_0 is the middle value of the distribution, conveniently, the mean, median, and mode. σ is, by definition, the standard deviation of the distribution. About 70% of the points in a Gaussian distribution are within one standard deviation of the mean. By comparing Figure 3.2 with Figure 3.3, it can be seen that a Gaussian distribution of similar height and normalized to the same area has much more of its area closer to its center than a Lorentzian. Their shapes are entirely different, and it is important to understand the shape of an absorbance peak when analyzing absorbance spectra.

In the case of IR-806, a monomer in solution may have a peak absorbance at a different wavelength than a dimer or other n-mer in solution. In this way, a particular Gaussian peak observed in a spectra can correlate with the presence of a certain type of aggregate species in solution. If IR-806 solution spectra change in such a way that it appears that a different gaussian peak contributes to the spectra, then that peak could represent the relative amount of a differently sized or shaped aggregate in the total population.

It is important that a certain "set" of peaks be used to represent all the spectra, independent of solution concentration. Similar to how a combination of n unit vectors in a basis set can represent all possible n dimensional coordinates in linear algebra a linear combination of peaks, each with a particular center and width, must be able to create the absorbance

spectra of each concentration. The amplitude of each peak varies depending on concentration and the relative change in amplitude reflects a change in the proportion of the n-mer in solution.

Therefore, the absorbance spectra of each IR-806 concentration was analyzed using a peak fitting computer program with gaussian distributions of fixed center, fixed width, and variable amplitude. The goal of this fitting was to find a uniform number of peaks, each with fixed center and width, for the spectra of all IR-806 concentrations, with only variation in peak amplitude. In this way, peak amplitude dependence on concentration would correlate with the trends of variously sized aggregate populations. In theory, at low concentrations, IR-806 monomer populations would dominate the absorbance spectrum. As the concentration increased, IR-806 aggregate peaks would account for the changing absorbance.

Ultimately, absorbance peak amplitude correlation with concentration can yield information regarding a self assembly mechanism. If there appears to be a set of peaks that can describe IR-806 absorbance spectra and the amplitudes of these peaks show a trend with concentration change, then various aggregation mechanisms can be investigated by fitting the theoretical equations from Section 2.3 to experimental absorption coefficient vs. concentration data.

Chapter 4

Experimental Results

4.1 Degradation

Results from IR-806 degradation pH dependence measurements are shown in Figure 4.1. Degradation rates for basic, neutral, and acidic solutions are quantified through their decay constants, also shown in Figure 4.1. Exponential decay functions were fit to all three data sets, and the exponential decay constants represent the amount of time required for the absorption to decrease from its initial value by a factor of e. Both the basic and neutral solutions were found to have decay constants about 100 hours. However the acidic solution was found to have a decay constant of only 20 hours.

Table 4.1: Exponential Decay best fit parameters

Solution Type (pH)	Decay Constant (hrs)
Acidic (2.8)	21 ± 1.6
Neutral (7.3)	108 ± 1.6
Basic (10.5)	101 ± 1.6

From these results, it is evident that IR-806 degradation in solution involves some interaction between the individual IR-806 molecule itself and hydrogen ions in solution. In experimental practice it was ensured that non-acidic solutions were created and experimented with at all times. Also, solutions were always created the same day they were used to ensure that no detectable degradation occurred beforehand.

4.2 Phase Diagram

Through the results of both the crossed polarizing microscope and the polarizer-laser apparatus two different phase diagrams were constructed. The microscope experiment provided qualitative observations about what IR-806's liquid crystal phase and phase transitions

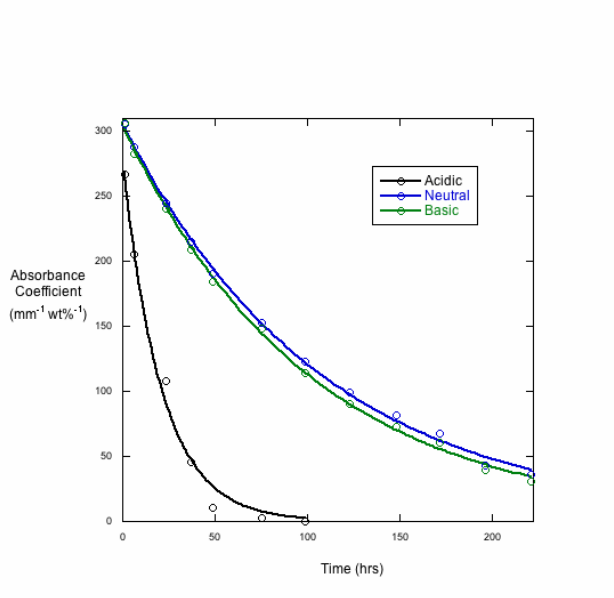

Figure 4.1: IR-806 absorbance degradation over time

looked like, while the laser experiment yielded quantitative results for the coexistence region and isotropic liquid transition temperatures.

4.2.1 Polarizing Microscope

Under the crossed-polarizer microscope, IR-806's liquid crystal phase appeared as very "textured," meaning that its domains of aligned aggregates were on a size scale to be discerned by the human eye under a magnification of 100x. Figure 4.2 shows a photograph of a 0.996 wt% IR-806 sample under crossed polarizers at room temperature. It is apparent that at such a high concentration, IR-806 is highly birefringent and its aggregates align into domains whose direction creates a very textured landscape. The dark areas under the slide are areas where the aggregates are aligned parallel to one of the polarizers and consequently do not change the polarization of the light that passes through them. These dark areas are still birefringent, as could be confirmed by rotating the microscope slide in relation to the crossed polarizers and observing their movement across the slide.

In all, a general trend was observed as temperature was increased for each IR-806 sample. From an observational standpoint, there were four major appearance changes. At the lowest temperatures (relative the sample concentration), IR-806 appeared similar in texture to Figure 4.2, with definite ridges and distinctly unaligned aggregate domains. However, as temperature increased, the texture became smoother, generally at a particular temperature, whereby the domains appeared to align on a macroscopic level and no ridges were observed under the microscope. At higher temperatures, the sample brightness began to decrease, continuously and uniformly, until no birefringence was observed. Even at the highest temperatures, some samples continued to show a faint birefringent streak across the slide, which

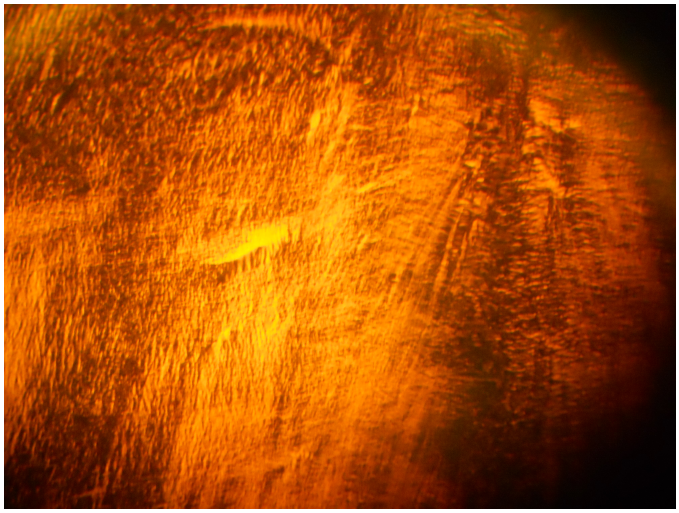

Figure 4.2: Liquid crystal 0.996 wt% IR-806 sample shown under a crossed polarizer microscope.

either went away at a much higher temperature, or remained because it outlasted the set upper bounds of the temperature run.

Table 4.2 shows the data from the microscope observations, with columns for sample concentrations (Conc.), the number of trials done at each concentration (Trials), and the average temperatures observed for the textural change (T_{text}), coexistence region onset ($T_{initial}$), coexistence region ending (T_{final}), and the final temperature where the birefringent streak went away (T_{streak}). No birefringent white streak remained after the coexistence region with 1.0 and 1.4 wt% sample, and no textural change was observed with the 1.0 wt% samples.

Table 4.2: Microscope Coexistence Region Observations

Conc. (wt%)	Trials	T_{text} (°C)	$T_{initial}$ (°C)	T_{final} (°C)	T_{streak} (°C)
0.4	2	17	25	38	50
1.0	3	n/a	35	45	n/a
1.4	1	27	43	53	n/a
2.0	3	45	52	58	80

From this data, a qualitative phase diagram for IR-806 was constructed, depicting the temperature ranges of the liquid crystal phase, coexistence and remaining white streak regions, and isotropic liquid phase depending on temperature. The birefringent white streak was not taken as part of the coexistence region in this diagram. Figure 4.3 shows the phase diagram below, with temperature as function of concentration for each of these four appearance changes under the microscope.

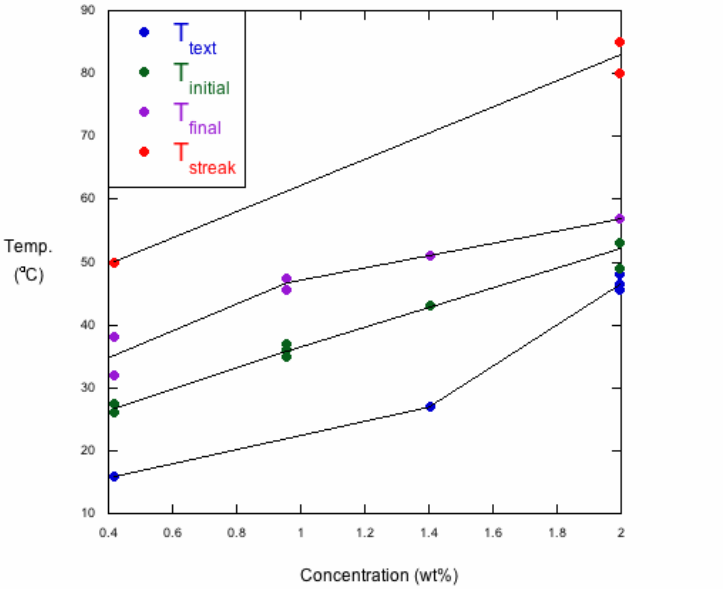

Figure 4.3: IR-806 phase diagram constructed from the polarizing microscope data, depicting qualitative physical changes of IR-806 samples depending on sample concentration and temperature.

4.2.2 Laser Apparatus

As it turned out, the crossed polarizer laser apparatus was necessary for obtaining a quantitative temperature range for IR-806's coexistence region. This is because IR-806's coexistence region has the unique quality of uniform and continuous decrease in birefringence, as opposed to a patchy coexistence region where large chunks of material spontaneously undergo transition into the liquid phase. Because IR-806 phase transition is marked by gradual birefringence dimming, no human eye can discern exactly when the dimming begins. Therefore, unbiased temperatures for IR-806 phase transition demanded quantitative measurements of light intensity detected through the sample as a function of temperature.

Because the lock-in amplifier could only measure the intensity of the light, the laser apparatus experiment could not provide any quantitative measurements regarding sample textural changes or the remaining birefringent streak observed in the microscope slides. As consequence, the phase diagram constructed from the laser apparatus data only provides information about IR-806's standard coexistence region. No information about IR-806's changing domains or birefringent white streak is quantitatively investigated.

However, the laser apparatus did provide means for a more precise and unbiased method in marking birefringence changes and provided a more reliable temperature range for coexistence regions of varying concentrations of IR-806. For each of these runs, a plot was

made of amplified voltage (proportional to light intensity) vs. temperature. When plotted the curve was broken up into linear segments, to model how the slope of birefringence vs. temperature would ideally change abruptly as consequence of a phase transition.

It is important to note that such a curve of light intensity vs. temperature of a liquid crystal is not common. Liquid crystal coexistence regions are commonly marked by an abrupt change in birefringence due to an immediate loss of all birefringence in a particular region of the sample. However, as mentioned in the microscope results, IR-806 shows uniform and continuous loss of birefringence in its coexistence region, which is quantitatively depicted through the curvature of Figure 4.4.

The steepest segment was labeled as the co-existence region segment, and the start and end temperatures for each co-existence region were determined by finding where the segment intersected with the liquid crystal and isotropic line segments (which were much shallower in slope). Due to such pronounced curvature, the transition temperatures for each concentration have an associated standard deviation of around 2 ℃. Although unconventional, the data analysis was systematic.

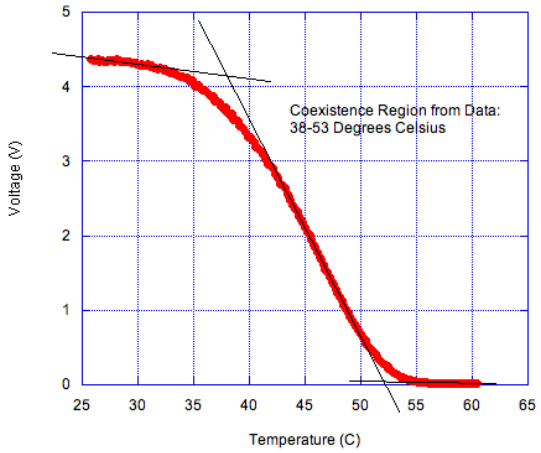

Figure 4.4: One example of a 2.0 wt% IR-806 laser run. The curvature of the data was not expected, and therefore extraction of the coexistence region temperature range required extrapolating the intersection of straight lines. In this way IR-806 phase transition was modeled by the behavior of previously studied liquid crystals.

A quantitative phase diagram was constructed from the laser apparatus results. The co-existence temperature range was as low as 10°C for the 0.4 wt% samples and as high as 15 °C for the 2.0 wt% samples. The compiled phase plot is shown below in figure 4.5.

4.3 Absorption Spectra

Absorbance measurements provide a plethra of new information. As concentration ranged from 0.0005-0.1 wt%, IR-806's absorbance spectra shifted from being dominated by an IR wavelength around 800nm to a lower wavelength around 680nm. As concentration increased,

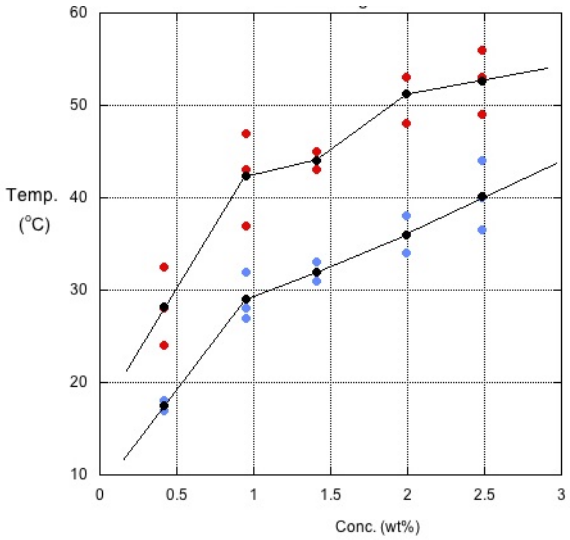

Figure 4.5: A phase diagram of IR-806 from the results determined by the crossed polarizer laser aparratus. The blue points correspond to coexistence region onset temperatures and the red points correspond to isotropic liquid phase onset temperatures. The dots are the average coexistence region initial and final temperatures for each concentration.

the 800nm peak decreased in height and gave rise to an increase in the 680nm peak height. At intermediate concentrations, IR-806 spectra are very interesting, showing a gradual transition in peak dominance, with higher absorbance at intermediate wavelengths.

Moreover, as concentrations increased from 0.1 wt%, IR-806 spectra further changed. At higher concentrations, absorbance spectra smoothly changed to incorporate a third peak, centered at an even higher wavelength of around 830nm. This peak, although located close to the low concentration peak, was much broader and consumed the general shape of the high concentration spectra. Indeed, the original 800nm peak quickly decreases in amplitude and becomes dwarfed by the 830nm peak in IR-806 concentrations above 0.25 wt%.

Figure 4 shows the range of low concentration data compared with range of high concentration data. On the left, concentrations range from 0.000499-0.101 wt%. On the right, concentrations range from 0.101-0.966 wt%. As can be seen, there appear to be three different peaks that dominate IR-806 spectra depending on the solution concentration. When observed under the cross-polarized microscope, the solutions with concentrations greater than 0.25 wt% were all observed to have at least some birefringence, which meant that they all had at least some aligned aggregates. It is exactly these concentrations that show the dominance of the third peak, which is redshifted.

Indeed, it does seem that IR-806 absorbance spectra peak amplitudes and centers might correlate with the presence of differently sized aggregates in solution. It also makes sense that the liquid crystal phase cannot occur until the appearance of a critically sized type of aggregate, and that the material quickly begins to align its aggregates after a certain amount of this aggregate type is formed.

Because the 800nm peak inversely correlates with concentration, it makes sense to label

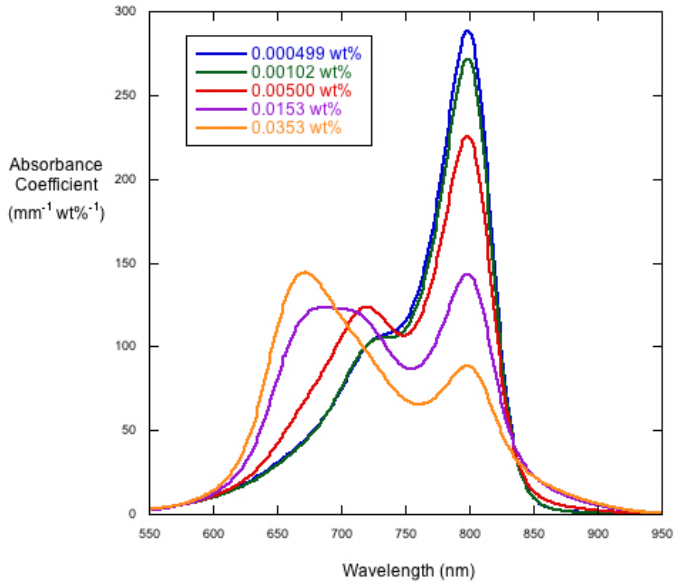

Figure 4.6: IR-806 Absorbance Coefficient vs. wavelength for low concentrations.

as the IR-806 monomer's signature absorbance. From here on out, the 800nm peak shall be referred to as the monomer peak. The presence of the 650nm peak is greatest among intermediate concentrations of IR-806 solution. Therefore, it likely correlates with the presence of an intermediate aggregate, larger than a monomer, but smaller, or differently shaped, than the large-scale aggregates that align to form the liquid crystal phase. In order to account for these options, the species responsible for this peak shall be referred to as an n-mer. Lastly, the 830nm peak is only present in high amplitude for the largest of IR-806 concentrations, where the solution is either in its coexistence region or liquid crystal phase. Therefore, we shall refer to it as the aggregate peak. It's presence dominates at concentrations where IR-806 is observed to enter its liquid crystal phase at room temperature. Thus, it makes sense that this is the signature peak of the aggregate responsible for IR-806's liquid crystal phase.

4.4 Peak Fitting

After many iterations of searching for the best set of peaks that, with fixed centers and widths, could represent all 14 experimental IR-806 absorbance spectra, it turned out that a total of six peaks were able to fit the data nicely. Table 4.3 shows the gaussian centers and standard deviation of each peak.

While only three of the peaks contributed to the changes in spectra by varying their peak

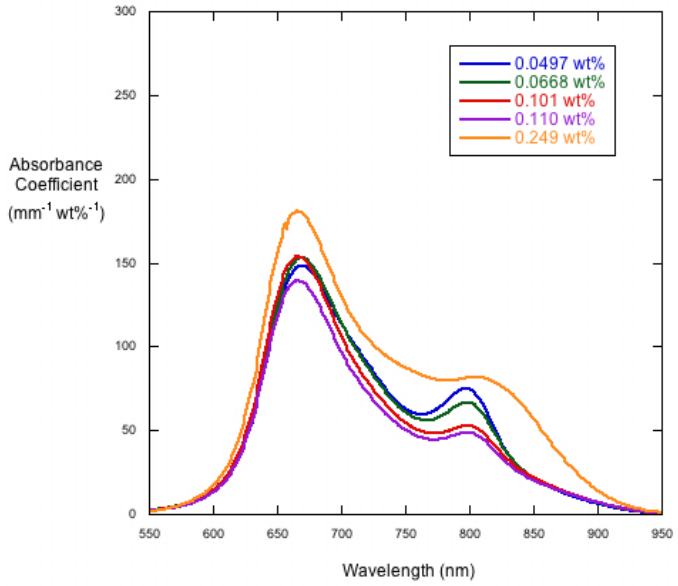

Figure 4.7: IR-806 Absorbance Coefficient vs. wavelength for middle concentrations.

heights, three additional peaks, of relatively constant amplitude, were needed to fill in the remainder of the absorbance spectra. Because these peaks are identical for all concentrations, their presence does not contribute to spectra changes, and it can be inferred that they are not related to the relative changes in IR-806 species in solution during aggregation.

The error in these measurement was estimated by comparing the final best fit peak parameters to best fit parameters of the near final fits. Personal decision-making was involved in this peak-fitting process, and, therefore, the errors in the final parameters are greater than the error values evaluated by the program itself. However, there is reassurance in the validity of this procedure from the fact that, for a given concentration, there was at least one parameter that was reasonably fixed. For example, the spectra for low concentrations of IR-806 fixed the 800 nm peak for high concentrations, and mandated that it have a small standard deviation. Likewise, measurements on high concentration IR-806 samples determined that a much broader peak exist around 830 nm, clearly different from the low concentration peak centered at 800 nm.

The amplitudes of the best fit aggregate peaks ranging through the various concentrations are plotted in Figure 4.9.

Three out of the six peaks are hypothesized to be either monomer or aggregate peaks. These correlate with the three distinct peak changes that were observed through IR-806 concentration variation. Peak 5 represents the monomer population, peak 2 represents the n-mer aggregate population, and peak 6 represents the aggregate structure. The amplitudes

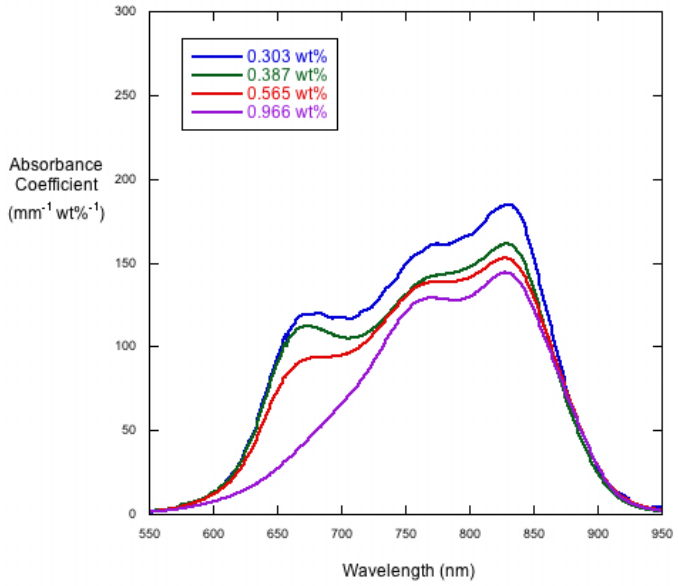

Figure 4.8: IR-806 Absorbance Coefficient vs. wavelength for high concentrations.

of peaks 1, 3, and 4 did not vary significantly with concentration, and are assumed for the time being to be intrinsic absorption properties of IR-806, independent of aggregation.

Figures 4.10-4.12 show the best fit peaks for three concentrations of IR-806. In Figure 4.10, the spectra and fit of a a 0.0005 wt% solution is overwhelmingly comprised by peak 5. In Figure 4.11, is modeled well by peak 2, but also has some contribution from peak 6. Peak 5 has significantly diminished. In Figure 4.12, peak 5 has vanished altogether, and the contribution of peak 2 has been almost entirely replaced by peak 6. Peaks 1, 3, and 4 have nearly the same contribution in all cases.

4.5 Aggregation Mechanisms

From the peak fitting results, different types of aggregation theories can be fit to the plots of peak amplitude vs. concentration. There are only three peaks whose amplitudes change, and only two of the peaks are substantially present for a given concentration. Up until about 0.12 wt%, the monomer peak decreases while the n-mer peak increases. There are two ways to model this trend.

First, we can think of this reaction as an IR-806 monomer undergoing a dimerization reaction to create a single product of IR-806 dimers in solution. This reaction is modeled through a standard chemical equilibrium, where two reactants are converted into a single

Table 4.3: Peak Fitting Gaussian Centers (λ) and Widths (σ)

Peak	λ (nm)	σ (nm)
1	630 ± 2	34 ± 8
2	667 ± 4	24 ± 8
3	716 ± 6	24 ± 10
4	759 ± 10	24 ± 6
5	800 ± 2	18 ± 3
6	828 ± 1	39 ± 10

product. The second way to model the monomer/n-mer data is by perceiving the increase in the amplitude of the $n-$mer peak from the population growth of a variety of small aggregates including, but not limited to, dimers in the solution. Within this low concentration range, only small aggregates are likely to be forming in solution, and they could all show a similar signature peak around 630 nm. Consequently, peak 2 could account for all of them. Whichever of these two theories best fits the data determines whether we should treat peak 2 as solely due to dimers, or view it as representative of a variety of small aggregates in solution.

While the aggregation theory discussed in Section 3.2 technically requires concentration units of molarity, we can use concentration units of weight fraction at sufficiently low concentration. This is because molarity and weight fraction only differ by a multiplicative constant, when the volume of the dye in solution is negligible compared to that of the solvent. Because the total dye concentration never exceeds a weight fraction of 0.01, using weight fraction as our units of concentration will only change our best fit equations by a factor of a constant. Moreover, because all components of the aggregation theory use the variable $L = K_E C_T$, we can actually fit the theory, unmodified in principle, to data where concentration is in weight *percent* instead of weight fraction. Although the conversion from weight fraction to weight percent introduces a factor of 100, the equilibrium constant can always absorb that multiplicative factor. Therefore, data analysis can, and is most easily done, in concentration units of wt $\%^{-1}$.

In order to construct the best fit equation for the dimerization equilibrium fit, we start with the general form of Equation 2.23 and omit the higher order terms beyond the dimer. From this, we can obtain an equation to represent the concentration of monomers in solution relative to total dye concentration. This equation is fitted to the monomer peak data. The n-mer fitting equation is just the monomer fitting equation subtracted from unity, as this theory accounts for *only* monomers and dimers as part of the mechanism. Table 4.4 shows the parameters for the best fit to this equation (K_E and m, the absorption parameter), and Figure 4.13 shows this fit plotted against the experimental data.

It can be seen from the fit that the monomer peak drops off too sharply for this theory. Moreover, the equilibrium constants calculated for each fit differ considerably, with of 1.3

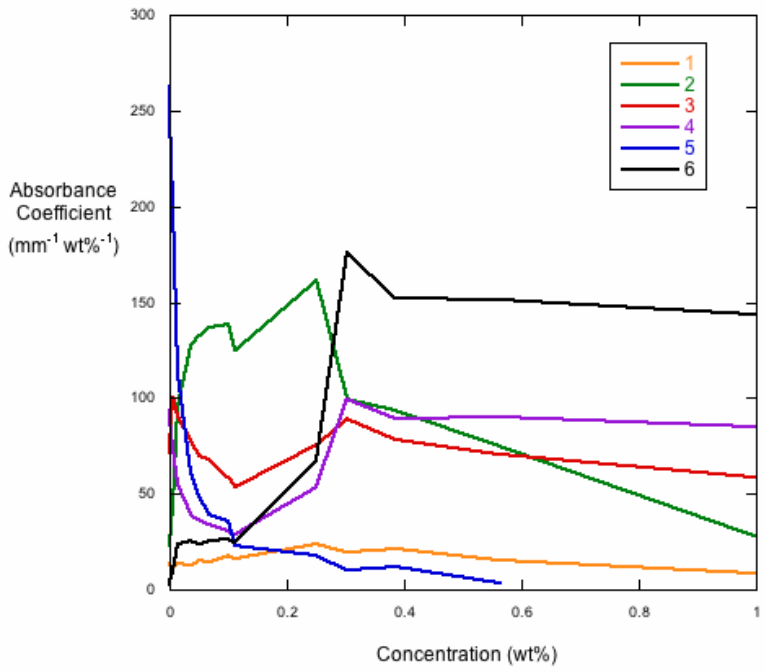

Figure 4.9: IR-806 aggregate peak amplitude dependence on concentration. Uncertainties for peaks 2, 5, and 6 are shown on Figures 4.13, 4.14, and 4.15.

standard deviations separating them. Therefore, we continue to isodesmic fitting to see if it can provide a better fit.

In the isodesmic fitting, we can refer back to Equation 2.27, where the isodesmic theory was derived. The monomer concentration fraction is given to us, and, as we are allowing the n-mer peak to account for other species in solution besides the dimer, we can again let the fit for the dimer peak be the monomer fitting equation subtracted from unity. We also provide a scaling factor that accounts for the absorption coefficient for the n-mers in solution.

Table 4.5 shows the parameters for the best fit to this equation, and Figure 4.14 shows this fit plotted agains the same experimental data.

It can be seen that the isodesmic fitting provides much better results than the dimerization equilibrium theory does. The best fit equilibrium constants for the monomer and n-mer curves are 58 and 56 $wt\%^{-1}$, which turns out to be less than a third of a standard deviation from one another. Moreover, the monomer fits the higher concentration data much more nicely than before.

For larger IR-806 concentrations, this isodesmic relation between solely monomer and intermediate aggregates loses its validity, because the larger aggregate concentration begins to rise. As concentrations increase, the monomer concentration decreases to near zero, and an interplay between the intermediate and aggregate populations dominates the scene. In this case, there is a more complicated mechanism, because the larger aggregate concentration remains very low until a critical point, at which it quickly increases to a maximum value. These results appear to be able to be modeled by a more cooperative mechanism, where,

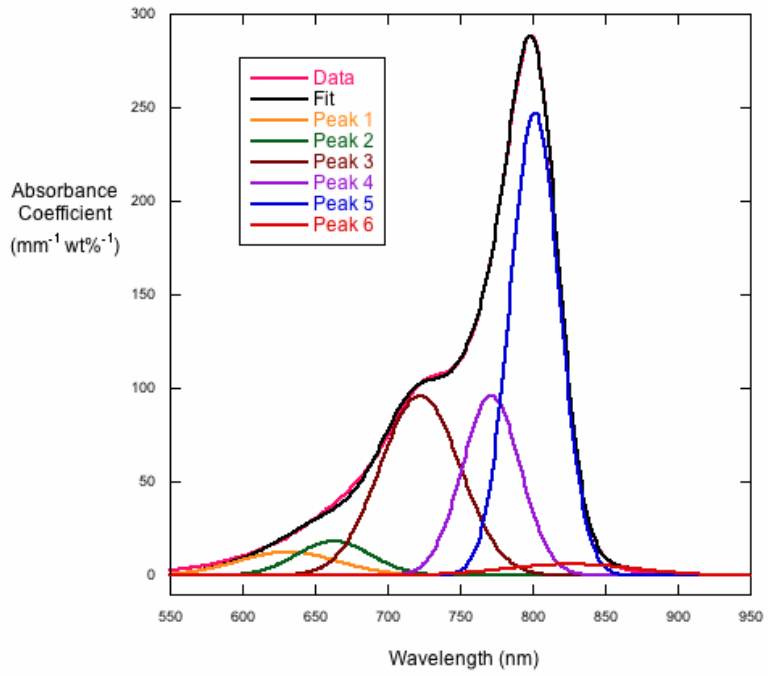

Figure 4.10: 0.000499 wt% Peak Fitting results.

instead of a uniform equilibrium constant existing between all the aggregate types in solution, the aggregate species has a lower equilibrium value that hinders its population until the IR-806 concentration reaches a critical threshold concentration. When this concentration is reached, formation of the aggregate becomes favorable, and the aggregate population can quickly increase.

The next simplest theory, beyond general equilibria or isodesmic modeling, is the use of an unequal K model, from Equation 2.29. This unequal K model is a type of cooperative mechanism, and, if it fits the data reasonably well, could suggest that the formation of large IR-806 aggregates is a hindered process that does not occur until a critical dye concentration. Because the monomer concentration is negligible at concentrations where the aggregate peak begins to rise, we shall use the amplitude of the n-mer peak to represent the the population of the reactants responsible for the reaction.

Figure 4.15 shows the fit for a cooperative assembly to the IR-806 results. The theoretical fit was plotted with the data in MatLab, whereby parameters were changed such that the curve fit reasonably well with the data. The best fit that kept the same equilibrium constant from the isodesmic fit beforehand, yielded an extremely small ρ value. This supports the notion that the formation of aggregates is a very hindered process and these larger aggregates can only form when the concentration exceeds a critical threshold that makes their formation more energetically favorable. However, since ρ was so small, K_E needed to be very large so that aggregation *would* continue after the concentration allowed for monomer formation. Although it is not a perfect fit, the curve matches the sudden rising of the larger aggregate's population in the solution.

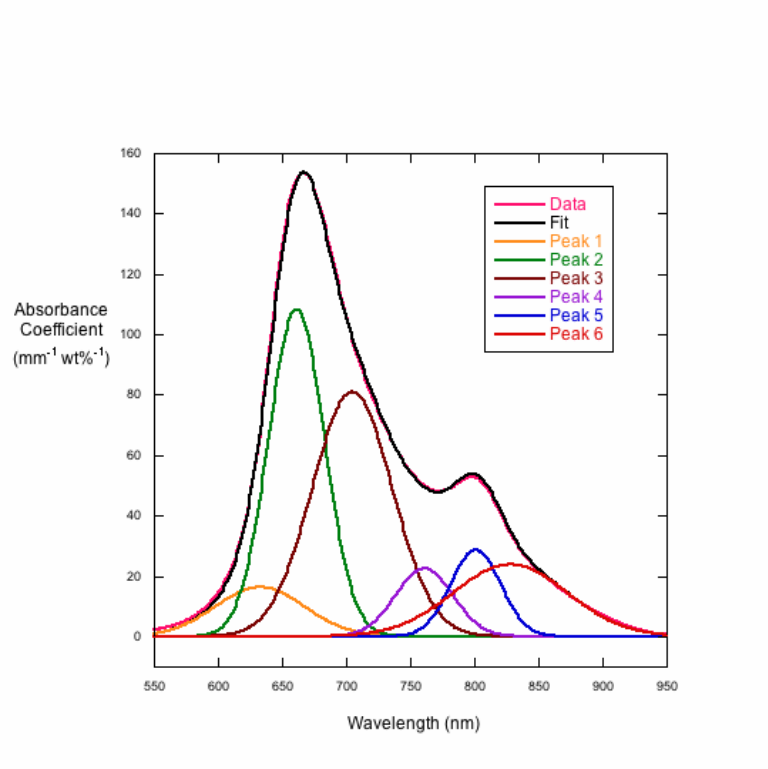

Figure 4.11: 0.101 wt% Peak Fitting results.

Referring back to Equation 2.32, there is no analytical solution to solving the Unequal K monomer dye fraction. Instead, a cubic equation must be solved numerically, with the smallest positive root being the solution. As such, a computer program was written to solve the equation for a range of concentrations, given an inputted equilibrium constant and value for ρ. From this, a list of monomer dye fractions could be generated and plotted. However, in order to fit the experimental data, a "best fit" equation needed to be generated via trial and error, testing values of K_E and ρ, and generating a χ^2 from the program to compare various fits. An additional two parameters were included, m and b, allowing for both a multiplicative factor and a vertical offset to the fit. These parameters allow for both the aggregate's absorbance coefficient and the fact that at these higher IR-806 concentrations, peak 6 already has a non-negligible amplitude (it's offset is twice the error). This presence suggests that there is already a small amount of aggregate species in lower IR-806 solution concentrations, but that it does not increase to a significant amount until a much higher total dye concentration is reached.

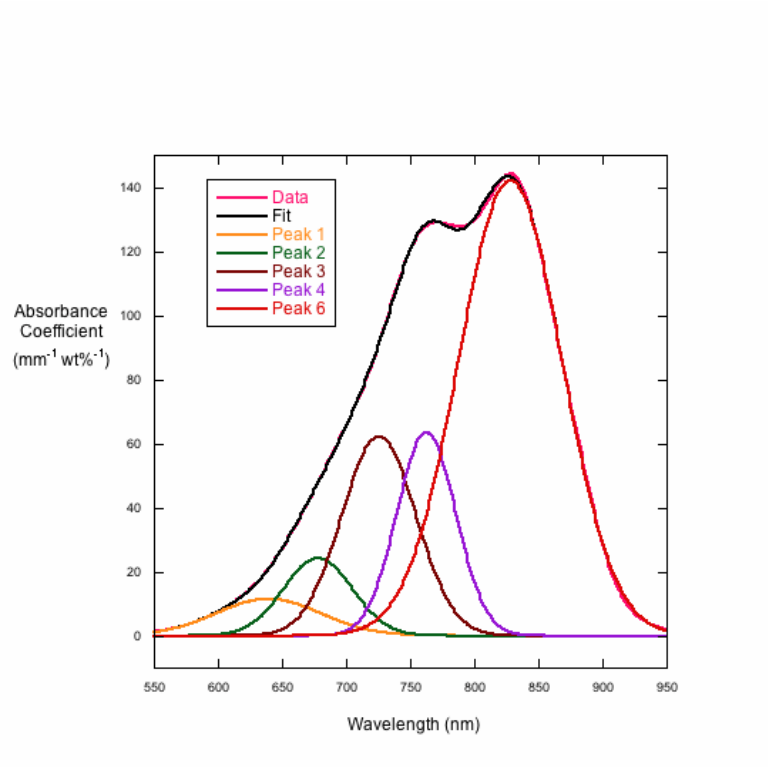

Figure 4.12: 0.996 wt% Peak Fitting results.

Table 4.4: General equilibrium fits and best fit parameters for Monomer/Dimer Data

Parameter	Monomer	Dimer
Equation	$m\left(\frac{(8K_EC_T)^{1/2}-1}{4K_EC_T}\right)$	$m\left(1-\frac{(8K_EC_T)^{1/2}-1}{4K_EC_T}\right)$
m	310 ± 32	190 ± 15
K_E	180 ± 78 wt%$^{-1}$	60 ± 19 wt%$^{-1}$
χ^2	2,635.7	523.63
R	0.97962	0.98585

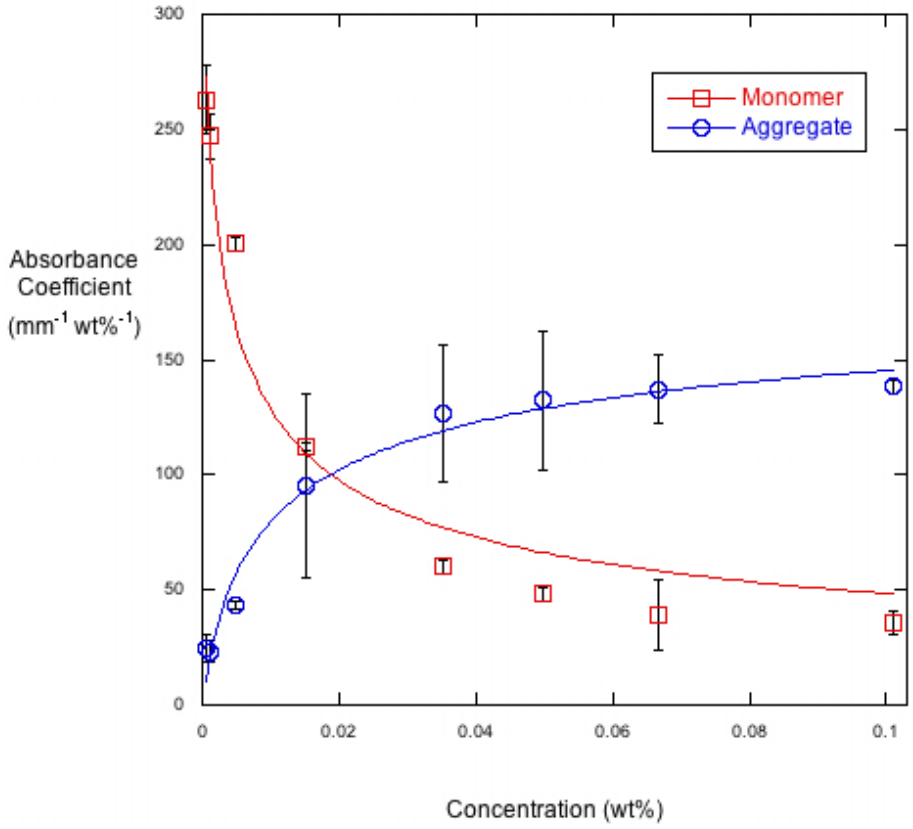

Figure 4.13: Dimerization equilibrium theory, fit to monomer and dimer experimental data. Table 4.4 shows the best fit equation and parameters for these data.

Table 4.5: General isodesmic fits and best fit parameters for Monomer/Dimer Data

Parameter	Monomer	Dimer
Equation	$m\left(\frac{2K_EC_T+1-\sqrt{4K_EC_T+1}}{2(K_EC_T)^2}\right)$	$m\left(1-\frac{2K_EC_T+1-\sqrt{4K_EC_T+1}}{2(K_EC_T)^2}\right)$
m	281 ± 7.9	162 ± 9.9
K_E	58 ± 6.2 wt%$^{-1}$	56 ± 15 wt%$^{-1}$
χ^2	460.66	490.88
R	0.99647	0.98674

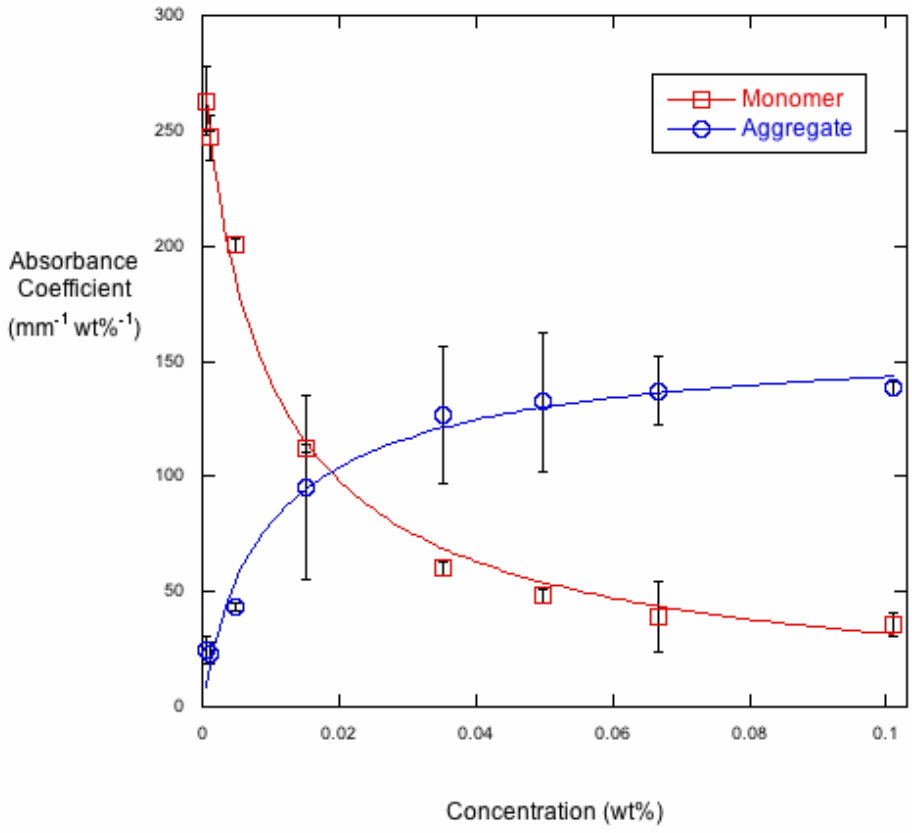

Figure 4.14: Isodesmic theory, fit to monomer and dimer experimental data. Table 4.5 shows the best fit equation and parameters for these data.

Table 4.6: Best Fit Unequal K Model Parameters for aggregate Data

Parameter	Value
m	170
b	25
K_E	790 wt%$^{-1}$
ρ	$1{*}10^{-7}$
χ^2	5,496.7

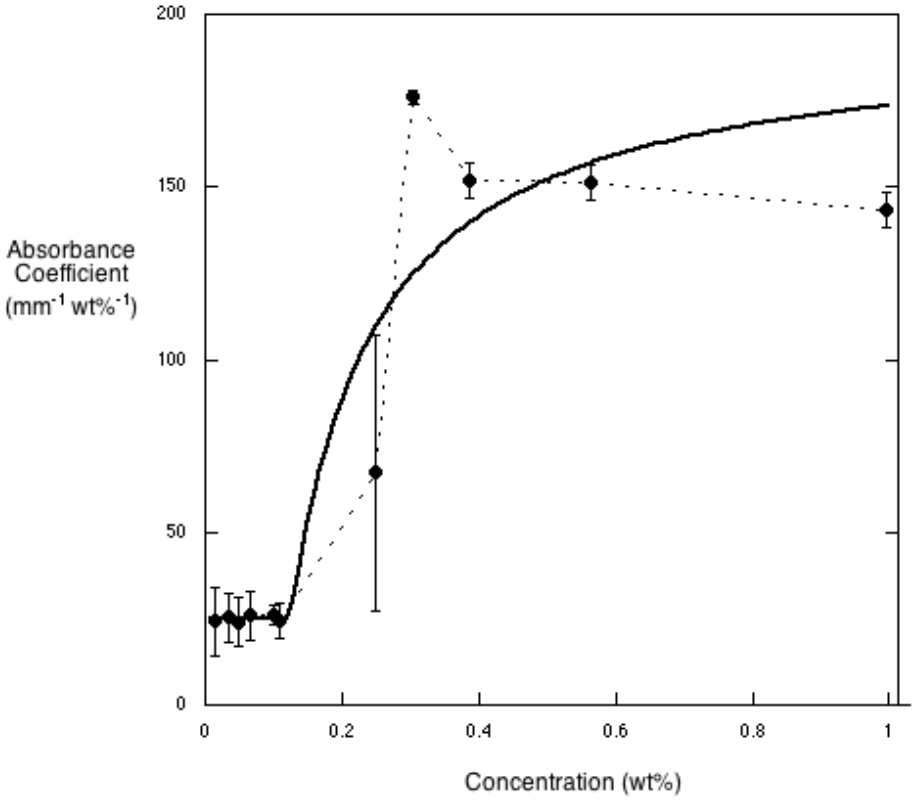

Figure 4.15: Best fit Unequal K curve plotted with aggregate experimental data. Table 4.6 shows the best fit equation and parameters for these data.

Chapter 5

Discussion

5.1 Degradation

While it cannot be said for sure *exactly* how IR-806 molecules degrade in solution, it has been found that solution acidity plays a large role in the process. While IR-806 cannot be made more stable, we *do* know how to maximize its stability and perform experiments with it before nontrivial degradation occurs. Since it degrades much more quickly in an acidic evironment, one is fine working with IR-806 in Millipore water, or even with an extremely low concentration of neutral buffer.

Also, lower concentrations of IR-806 degrade more quickly than higher concentrations. However, even IR-806 in liquid crystal phase eventually loses both its vibrant hue and birefringence. This means that IR-806's structure dramatically changes as it interacts with water over a period of time.

This information could help to explain how IR-806 interacts with the other molecules around it in solution, specifically if IR-806 molecules interact uniquely with water, and potentially in such a way that could influence aggregation structure and mechanism.

However, from a research perspective, IR-806 in pH 7 solution is stable for at least several hours, and as long as experiments are carried out in a timely fashion, all results can be analyzed assuming minimal molecular degredation.

What is perhaps more interesting to think about is what intramolecular interaction are occurring within the structure of IR-806 molecules involving acidic water based solutions and lead to the destruction of the molecular visible light absorption properties. There are several types of chemical reactions that could be occurring, and investigation of these reactions could shed light on how IR-806's structure interacts with water, perhaps in a similar way that it does when it is in an aggregate structure.

5.2 Phase Diagram

A precise measurement and display of transition temperature vs. concentration were obtained for IR-806. However, minimal quantitative measurement was gained about the pos-

sible "smoothing" factor for temperatures below the the co-existence region temperatures. While smoothing was observed for some samples when heated under the microscope, the laser apparatus did not detect any smoothing because the smoothing did not substantially change the intensity of the light emerging through the sample.

IR-806's phase diagram is comparable to that found for BPP. However, it is important to note that IR-806 does form its liquid crystal phase at a lower concentration than BPP. It would be interesting to test IR-806's liquid crystal properties at even higher concentrations than 2.5 wt%, but practical limitations arise from IR-806's extremely high viscosity and surfactant nature at concentrations as low as 1 wt%.

Figure 5.1 shows the phase diagram for BPP, which can be compared to the that previously shown for IR-806.

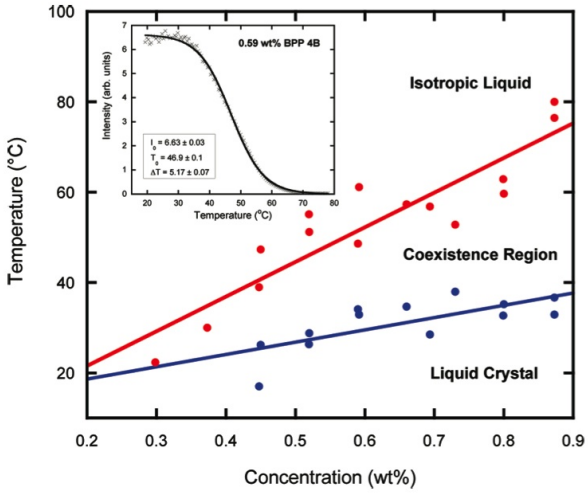

Figure 5.1: Phase diagram for BPP, shown with an example run in the crossed polarizer laser apparatus. [8]

Through these data and IR-806 phase transition experimentation, the most important connection between IR-806 and BPP has been found to exist between the *way* in which their coexistence regions occur. *Both* coexistence regions have been observed to uniquely change uniformly through the sample. While the coexistence regions in DSCG, Sunset Yellow, and Bordeaux dye can easily be detected under a microscope from the separation of large birefringent and isotropic domains, IR-806 and BPP do not provide an easy means for observationally detecting their coexistence regions. Their coexistence regions are observed as a uniform reduction in birefringence throughout the entire sample. The phase transition from orientational order to complete disorder does not occur in clusters large enough to discern under a microscope.

One possible explanation for why IR-806 and BPP have such a different type of phase transition from other chromonic liquid crystals, is that their liquid crystal and isotropic liquid phases could be very similar in physical properties, creating less of a driving force for separating the birefringent and isotropic groups of aggregates from one another. Chromonics

like DSCG and Sunset Yellow exhibit coexistence phases where aggregates transition in large patches, so as to minimize the surface tension between the isotropic and liquid crystal phases. Surface tension is frequently defined as force per unit length, which is useful when considering how a needle can float on the surface of a liquid when the liquid around the needle feels a strong enough attractive force to stay bonded to its neighboring liquid molecules, to combat the force of gravity, which is greater on the needle (from its larger density). However, surface tension can also be conceptualized as energy per unit area (and in this case is often referred to as surface *energy*, and it is more useful to think of it in this light when considering an interface between two materials in solution). Just as water is frequently attracted to itself more than it is attracted to other substances, so too are aligned aggregates in a liquid crystal phase transition attracted more to other aligned aggregates than disordered ones. This preference is energetically driven from the fact that aligned aggregates take up less volume and have more degrees of freedom when next to aligned aggregates, as opposed to randomly oriented aggregates. This is the same reason why the aggregates align into the liquid crystal phase in the first place. Therefore, as a chromonic liquid crystal transitions from its liquid crystal phase into an isotropic phase, the aggregates that begin to lose their alignment in solution wind up being next to other unaligned aggregates. On a macroscopic level, a DSCG or Sunset Yellow sample in its phase transition under a polarizing microscope appears to have spherical blobs of isotropic region within an overall birefringent region, with the isotropic spheres growing as temperature increases. This minimizes the surface area of the liquid crystal-isotropic liquid interface for a given volume of material in the isotropic liquid phase. Eventually, the isotropic spheres coalesce, and engulf the birefringent region as the sample becomes entirely isotropic liquid.

However, if aligned aggregates of IR-806 and BPP do not have a strong preference between residing next to other aligned aggregates or unaligned aggregates, then many small patches of isotropic liquid regions can exist intermingled among aggregates still in the liquid crystal phase. If the isotropic patches remain smaller than the resolution of the microscope (about a μ m), they are too small to be seen. In this case, the coexistence region would be observed as merely an overall decrease in birefringence (as the number of small isotropic patches increases), without any indication regarding which parts of the sample transition at a given point in time. This is exactly the result we observed.

5.3 Absorption Spectra

Overall, the absorption spectra component of IR-806 research has been a huge success. The absorption coefficient spectra of IR-806 concentrations have been mapped to the relative populations of variously sized aggregate species in the solution. This has paved the way for peak fitting and ultimately testing of IR-806 aggregate self-assembly mechanisms. IR-806 absorption coefficients spanning 500-1000 nm in wavelength and 0.0005-1.0 wt% in concentration have been accurately measured, and these data are being used for further investigation into IR-806 aggregation.

Moreover, IR-806 has a changing absorption spectrum that is similar to PIC. Although

the aggregate peak is not as narrow as the monomer peak, it does occur at a higher wavelength and could represents an "offset" stacking of the IR-806 molecules in an aggregate structure. Also, the aggregate peak does have a lower absorption coefficient than the monomer peak, just like PIC's aggregate peak. This reduction in peak amplitude is thought to occur because of near neighbor effects whereby multiple molecules are all contributing as "one" to the absorption characteristics of the material.

However, IR-806 is not exactly like PIC, and it is important to remember how they are different. PIC's aggregate peak is much narrow than its monomer peak, which is *not* the case for IR-806. Clearly, there is a difference between their aggregate structures that makes their aggregate widths so different from one another. In contrast, IR-806's *monomer* peak is far thinner than all its other absorbance peaks.

It is also important to recognize the possibility for error in the large concentration absorbance measurements, as there is no *proof* that thickness of the thin slides was calibrated properly. The best available process was used, and it appeared to work, but there is always the possibility that slide thicknesses were not identical to to their calculated thickness. Such uncertainty propagates through peak fitting analysis and fitting theory to aggregation mechanisms, in that peak amplitudes may not be entirely accurate for the highest IR-806 concentrations.

5.4 Peak Fitting

IR-806 peak fitting was successful, and results showed three peaks, in particular, that respectively represented the populations of different species types in solution. It is logical to consider peak 5 as representative of the monomer population, and peak 6 as representative of the liquid crystal aggregate population. Because an isodesmic theory fit the amplitudes of peaks 5 and 2 vs. concentration much better than a dimerization equilibrium did, peak 2 is most likely representative of a range of small n-mer aggregates. Moreover, the presence of three constant peaks through all concentrations suggests that the monomer has a component to its absorbance spectra that remains constant throughout all of its aggregation, including the liquid crystal phase.

The theoretical fits for isodesmic and cooperative aggregation, provide valuable information. While we still do not know the size of the observed aggregate species, we do know that the monomer and intermediate aggregates interact in an isodesmic fashion at low concentrations. However, the formation of the large aggregate at higher concentrations is likely to be involved in a cooperative system. Indeed, it appears that formation into the large aggregate is not energetically favorable until the concentration has increased such that these large aggregates can align and form the liquid crystal phase. It was observed that the formation of the large aggregate peak in the absorption data started at concentrations very close to the coexistence region of IR-806.

Moreover, we can obtain a stacking free energy change for IR-806 and compare this value to the other chromonics. Using the equation

$$K_E = e^{\Delta\mu/k_BT}, \tag{5.1}$$

we can calculate the stacking free energy change from our monomer/n-mer mechanism equilibrium constant. In this equation, $\Delta\mu$ is the change in chemical potential, or molar Gibbs Free Energy change. As currently stands, the equilibrium constant is in units of inverse weight percent, which can easily be converted to weight fraction. However, convention stands to use dye fraction concentration in units of *volume* fraction, so this equilibrium constant must be converted from inverse weight fraction to inverse volume fraction. This unit conversion would be a little nasty, save for the fact that we are working with solutions with relatively low total dye concentration. While the exact relation between volume fraction and mass fraction is:

$$\text{weight fraction} = \frac{m_{\text{dye}}}{m_{\text{dye}} + m_{\text{H}_2\text{O}}} = \frac{V_{\text{dye}}\rho_{\text{dye}}}{V_{\text{dye}}\rho_{\text{dye}} + V_{\text{H}_2\text{O}}\rho_{\text{H}_2\text{O}}}, \tag{5.2}$$

at low enough concentrations where they volume of dye is negligible compared to the volume of solvent in the solution. Therefore, the dye term in the denominator of the equation can be regarded as negligible, and the entire equation reduces to:

$$\text{mass fraction} = \frac{V_{\text{dye}}\rho_{\text{dye}}}{V_{\text{dye}}\rho_{\text{dye}} + V_{\text{H}_2\text{O}}\rho_{\text{H}_2\text{O}}} = \frac{V_{\text{dye}}\rho_{\text{dye}}}{V_{\text{H}_2\text{O}}\rho_{\text{H}_2\text{O}}} = \frac{\rho_{\text{dye}}}{\rho_{\text{H}_2\text{O}}} * \text{volume fraction}. \tag{5.3}$$

In these equations, m is the mass and ρ is the mass density of the dye and solvent. Because absorbance measurements were taken at room temperature, we can estimate the density of water as 1 g/mL. Therefore, at low concentrations, the conversion between weight fraction and volume fraction is a factor of the dye mass density. Currently, most chromonics are estimated to have a density of around 1.4 g/mL in low concentration solution, so that is our estimate for IR-806 dye. [5] Therefore, an equilibrium constant of 5800 inverse weight fraction converts to 8120 inverse volume fraction, and gives a stacking free energy of $9.01 \pm .12\ k_BT$.

The error associated with this calculated was determined by propagating the error from the best fit equilibrium constant, where

$$\sigma_{\Delta\mu/K_BT} = \frac{\partial\Delta\mu/K_BT}{\partial K_E}\sigma_{K_E} = \frac{\sigma_{K_E}}{K_E}. \tag{5.4}$$

This stacking free energy change associated with the mechanism for IR-806 aggregation is around the stacking free energies found for other chromonics, with a value lower than BPP's and around the same range as that calculated for Bordeaux dye. Therefore, there is a significantly strong drive for low concentration aggregation of monomers into dimers and other small n-mers in solution. However, as shown in the high concentration data fitting,

there is a significant hindrance in forming large IR-806 aggregates. It appears that there needs to be a critical total dye concentration before the large aggregates responsible for the liquid crystal phase transition begin to form.

It is important to recognize that peak fittings on their own do not provide information about aggregate size. Therefore, no declarations can be made about the exact size or structure of the aggregates observed through IR-806's changing absorption spectra. Instead, aggregate structures can only be inferred based upon the known concentration of the dye that correlates with the presence of each peak. There is the possibility that aggregates differing only by a few molecules have nearly identical absorbance spectra, or spectra with certain peaks slightly broadened or shifted. We accounted for this possibility with peak 2, by allowing it to include various n-mers, but we have not considered the fact that IR-806 *monomers* in solution could exhibit spectra properties very similar to dimer and other small n-mers. This would mean that peak 2 would be more representative of a variety of *larger* aggregates in solution and that peak 5 would be the one that represented a small group of n-mers that *included* the monomer population. This would require a change in the theory, as peak 5 does not represent a *sum* of aggregate populations in our analysis. However, while these alternative scenarios are possible, it is reassuring that the isodesmic aggregation theory worked well with the low concentration data, and appears to be a viable explanation for the low concentration aggregation reaction.

Also, it is interesting that the amplitude of peak 6 *decreases* at the highest concentrations, where IR-806 is in its liquid crystal phase. There are a number of reasons why this could have been observed. First, it could be that IR-806 aggregates undergo a third reaction to form a different structure, with a new signature peak, at even higher concentrations. Second, the absorbance coefficient of the aggregates might change when they align into the liquid crystal phase, due to the polarizing effects in the spectrophotometer. The decrease in peak 5 amplitude occurs right around this area, so this is a highly plausible theory. Or, it could be residual error from the initial uncertainty in the hand-made slides used to obtain the high concentration absorbance data. Higher concentration absorbance measurements of IR-806 might shed light on this matter.

Chapter 6

Conclusion

6.1 Future Experiments

6.1.1 X-Ray Diffraction

Preliminary x-ray diffraction measurements on 0.5 wt% and 1.0 wt% IR-806 samples have suggested that there is no repeat distance in either the dimension of molecular stacking or distance between aggregate structures in the liquid crystal phase. Such results support the notion that IR-806 aggregates very differently than previously studied chromonics like DSCG, Sunset Yellow, and Bordeaux Dye. If IR-806 aggregates are not comprised of single molecule "stacks" and the overall aggregates are wider than several molecular diameters, then there is no way x-ray diffraction can detect a repeating pattern in the structure. BPP was also found to have too large a distance between its aggregates to be detected by x-ray diffraction.

A second interpretation for such x-ray diffraction results refers back to IR-806's interesting coexistence region. There is a possible aggregate structure that would give both the observed uniform coexistence region and lack of x-ray diffraction detection. If individual molecules created a thin cylindrical veneer that encapsulated water molecules within the structure, the overall electron density of of the aggregates would not be very different from the surrounding water molecules. Since x-ray diffraction looks at repeating units of electron/photon scattering on the order of the incident photon's wavelength (Å), there would be no detection of such a repeating unit.

However, one must also be wary of the fact that x-ray diffraction was done on such low concentrations of IR-806 dye. The x-ray diffraction signal depends on the density of the repeating pattern in solution, and, in comparison to the liquid crystal phase concentrations of other chromonics, there is *very* little IR-806 to induce scattering in the solution. If more tests are done with higher concentration, it may be possible to determine whether there *is* a repeating pattern in IR-806's aggregate structure, or if the aggregates really do have an entirely unknown configuration of molecules and, perhaps, even include water in their structure.

6.1.2 Dynamic Light Scattering

Dynamic light scattering (DLS) is an experimental technique that measures the various sizes of particles in solution by means of scattering incident radiation off them and measuring their rate of diffusion (which inversely correlates with size). A wavelength of light with low absorbing properties is used, and, if particles are larger than a micron in solution, they are detected by the scattering light. Preliminary DLS measurements on a variety of IR-806 concentrations have presented puzzling results. When IR-806 solutions are prepared in filtered (0.2 µm) Millipore water, large structures are detected for *all* concentrations, including concentrations as low as 0.005 wt%. However, when solutions are filtered *after* they are created, *none* of the concentrations appear to contain any objects. At the same time, filtered IR-806 concentrations greater than 0.3 wt% still appear at least somewhat birefringent under the polarizing microscope, indicating that aggregates are present and form a liquid crystal phase.

It would be interesting to perform more DLS experiments, with both filtered and unfiltered IR-806 solutions, with greater care taken to completely dissolve IR-806 molecules as much a possible in the solution. There is a possibility that IR-806 molecules form complex structures when the power dye initially comes into contact with water. In order to dissolve the dye in solution more thoroughly, solutions can be vortexed with heat for a greater length of time, or even sonicated.

However, given that high concentration filtered samples were birefringent, there must be aggregates present in the experiment large enough to align into a liquid crystal phase. This finding provides another source of support for a unique aggregate structure. Because DLS relies on scattering of light off the interface between two media, it only works when there is a large change in refractive index between the solvent and particle in solution. Therefore, if the aggregates really are comprised of mostly water with only a thin cylindrical covering of IR-806 molecules, then, at our wavelength of light ($\sim$ 500 nm), there is minimal change in refractive index at the aggregate surface, and little scattering.

In order to test this possibility, a sample of IR-806, in its coexistence region can be sealed airtight between a coverslip and microscope slide (similar to the process described for the crossed-polarizer laser experiment in Section 3.2.2), and observed over the course of several days. There is a chance that two phases in the coexistence region might separate if given a long enough amount of time, and this would show that IR-806 just has a *weak* driving force for this phase separation. If no separation were observed over a course of days, the sample could be inserted in a centrifuge. Perhaps the slight difference in density between the two phases would cause them to separate, and then the separated phases could be observed under a polarizing microscope.

6.1.3 Other NIR Dyes

While IR-806 is the first known chromonic liquid crystal that has both a mechanistic signature to its absorption spectra and a continuous coexistence region, there are many other infrared absorbing dyes on the market with similar molecular properties. Many of these

have been shown to aggregate, and it would be interesting to see if some of them form a liquid crystal phase at high enough concentration. Most IR dyes are used as biological chromophores (fluorescing tags that use lower energy light as to not disturb the neighboring cell material), so they are currently being analyzed in a very low concentration. Perhaps a different IR absorbing dye can be found with similar absorbance and liquid crystal properties as IR-806, one that is more stable in solution than IR-806 and has the potential for more practical applications.

6.2 Final Thoughts

IR-806 does seem like a bizarre chromonic liquid crystal, but, in all, it does have birefringence and therefore the current definitions accepted and characteristics of these materials must be expanded to include it. Moreover, its discovery and analysis may pave the way for a whole new type of chromonic liquid crystal and shed light on the aggregation mechanisms of previously studied chromonics and those currently under investigation. We have learned much about the IR-806 structure, degradation, and absorbance spectra. While it is frustrating that such a molecule degrades over time, this degradation has been characterized, and steps have been taken to ensure that such degradation does not interfere with experimentation. In the larger sense, however, IR-806 will always be limited in its applications because of its instability in solution.

Also, IR-806's lowest energy gas phase molecular conformation has been determined in monomer form. However, it is likely to form an aggregate with a more complicated structure than just stacking, and it is likely that IR-806 molecules interact with water when the are in both monomer and aggregate form. Therefore, this conformation may not be the most stable form when such polar interactions are included. But, we know that there would need to be a very strong external/intermolecular driving force for IR-806 to exist in a conformation other than its AA state. Water and aggregate interactions would need to *favor* a different conformation considerably more than AA. It is unlikely that steric hindrance could be negated by *adding* more molecules to the equation.

It is extremely interesting, though, that IR-806's absorbance spectra changes so dramatically with concentration, and it is one of a few chromonic liquid crystals of its kind that has such strong correlation between its absorption and aggregation properties. The fact that IR-806's aggregation appears to shift from an isodesmic to a more cooperative mechanism is evidence for a structural change of the aggregate between intermediate and high solution concentrations. Moreover, after the high concentration aggregates are formed, it takes only a slightly higher concentration to align them into a liquid crystal phase. Such understanding can help us learn about the aggregation process of other chromonics when their absorbance spectra cannot provide enough information.

Acknowledgments

First, I would like to thank Swarthmore's Physics and Astronomy and Chemistry Departments. My professors and classmates are brilliant, authentic, and a consistent source of motivation for me. Specifically, I thank Carl Grossman, Kathleen Howard, David Trimble, and Liliya Yatsunyk for their time, equipment, and inspiration. I especially appreciate Paul Rablen's help in performing the Gaussian energy optimizations and his collaboration throughout the year.

I thank Sigma Xi, the American Chemical Society - Petroleum Research Fund, the Howard Hughes Medical Institute, and the National Science Foundation for supporting my work these last two years. I also thank Andrew McGhie, the UPenn REU program, and the Laboratory for Research on the Structure of Matter for exposing me to new types of exciting research for my future.

I send thanks out to Erik Smith and Ben Yelsey for being awesome lab partners who taught me so much. I also am indebted to the students whose research has paved the way for mine, and I thank all the liquid crystal theses writers for their example.

I extend my final thank you to my advisor, Peter Collings, whose wisdom and patience has helped me become the student and person I am. Peter has been such a mentor and role-model for me, and I will always appreciate my liquid crystal research with him.

Bibliography

[1] P. J. Collings, *Liquid Crystals: Nature's Delicate Phase of Matter*, Princeton University Press, second edition, 2007.

[2] L. Vicari, *Optical Applications of Liquid Crystals*, IOP Publishing Ltd, London, first edition, 2003.

[3] P. J. Collings and M. Hird, *Introduction to Liquid Crystals: Chemistry and Physics*, Taylor and Francis Ltd, first edition, 1997.

[4] D. Voet, J. G. Voet, and C. W. Pratt, *Fundamentals of Biochemistry: Life at the Molecular Level*, Wiley and Sons, Inc., Hoboken, third edition, 2008.

[5] M. R. Tomasik and P. J. Collings, J. Phys. Chem. **112**, 9883 (2008).

[6] P. J. Cragg, *Supramolecular Chemistry: From Biological Inspiration to Biomedical Applications*, Spring Science and Business Media, first edition, 2010.

[7] J. Lydon, J. Mater. Chem. **20**, 10071 (2010).

[8] C. B. M. et al., J. Phys. Chem. **114**, 1888 (2010).

[9] J. Lydon, Current Opinion in Colloid and Interface Science **8**, 480 (204).

[10] A. G. S. et al., Langmuir **20**, 6988 (2004).

[11] X. Song and J. W. Foley, Dyes and Pigments **78**, 60 (2008).

[12] T. Engel and P. Reid, *Physical Chemistry*, Pearson Education, Inc. Upper Saddle River, NJ, second edition, 2006.

[13] Gaussian 09, Revision A.02, M.J. Frish, G. W. Trucks, H. B. Schlegel, G. E. Scuseria, M. A. Robb, J. R. Cheeseman, G. Scalmani, V. Barone, B. Mennucci, G. A. Petersson, H. Nakatsuji, M. Caricato, X. Li, H. P. Hratchian, A. F. Izmaylov, J. Bloino, G. Zheng, J. L. Sonnenberg, M. Hada, M. Ehara, K. Toyota, R. Fukuda, J. Hasegawa, M. Ishida, T. Nakajima, Y. Honda, O. Kitao, H. Nakai, T. Vreven, J. A. Montgomery, J. E. Peralta, F. Ogliaro, M. Bearpark, J. J. Heyd, E. Brothers, K. N. Kudin, V. N. Staroverov, R. Kobayashi, J. Normand, K. Raghavachari, A. Rendell, J. C. Burant, S. S. Iyengar, J.

Tomasi, M. Cossi, N. Rega, J. M. Millam, M. Klene, J. E. Knox, J. B. Cross, V. Bakken, C. Adamo, J. Jaramillo, R. Gomperts, R. E. Stratmann, O. Yazyev, A. J. Austin, R. Cammi, C. Pomelli, J. W. Ochterski, R. L. Martin, K. Morokuma, V. G. Zakrzewski, G. A. Voth, P. Salvador, J. J. Dannenberg, S. Dapprich, A. D. Daniels, O. Farkas, J. B. Foresman, J. V. Ortiz, J. Cioslowski and D. J. Fox, Gaussian Inc., Wallingford CT (2009).

[14] A. D. Becke, J. Chem. Phys. **98**, 5648 (1993).

[15] W. Y. C. Lee and G. R. Parr, Phys. Rev. B **37**, 785 (1988).

[16] H. S. B. Miehlich, A. Savin and H. Preuss, Chem. Phys. lett. **157**, 200 (1999).

[17] P. v. R. S. W. J. Hehre, L. Radom and J. A. Pople, *Ab Initio Molecular Orbital Theory*, Wiley, New York, first edition, 1986.

[18] D. J. Griffiths, *Introduction to Electrodynamics*, Pearson Education Inc., third edition, 1999.

[19] R. B. Martin, Chemical Reviews **96**, 3044 (1996).

[20] M. M. J. Smulders, Chem. Eur. J **16**, 362 (2010).

[21] Z. C. et al., Chem. Soc. Rev. **38**, 564 (2009).